MASTER IN ASTROPHYSICS AND SPACE SCIENCE

Erasmus Mundus Master
in Astrophysics and Space Science

Master Thesis

Lensing and Photon Rings in a Magnetized Black Hole Spacetime.

Supervisors

PD Dr. Volker Perlick
University of Bremen, Germany

Prof. Predrag Jovanovic
University of Belgrade, Serbia

Author

Muhammad Haider Khan

Academic Year 2024/2025

TOR VERGATA UNIVERSITÀ DEGLI STUDI DI ROMA · UNIVERSITY OF BELGRADE · University of Bremen · UNIVERSITÉ CÔTE D'AZUR · Co-funded by the European Union

This Master thesis is submitted in partial fulfillment of the requirements for the degree The Erasmus Mundus Joint Master's Programme in Astrophysics and Space Science (MASS) as part of a multiple degree awarded in the framework of the Erasmus Mundus Joint Master in Astrophysics and Space Science - MASS jointly delivered by a Consortium of four Universities: Tor Vergata University of Rome, University of Belgrade, University of Bremen, and Université Cote d'Azur, regulated by the MASS Consortium Agreement and Co-funded by the EU under the call ERASMUS-EDU-2021-PEX-EMJM-MOB.

Contents

Abstract

The study of geodesics around black holes is fundamental in understanding gravitational lensing, shadow formation, and astrophysical processes near compact objects. In this work, we investigate lightlike geodesics in the Ernst spacetime (Schwarzschild-Melvin black hole), which describes a Schwarzschild black hole immersed in an external uniform magnetic field. The presence of this magnetic field B modifies light rays' trajectories, leading to significant changes in the structure of photon geodesics compared to the standard Schwarzschild case.

We work with lightlike geodesics in the Ernst spacetime and obtain conditions for circular lightlike geodesics in the equatorial and meridional planes. Using the Hamiltonian formalism, we derive a cubic equation in the radial coordinate r, whose solutions determine the possible radii of circular photon orbits about the z-axis. Our analysis reveals that such orbits are only possible in the equatorial plane, while we identify a critical magnetic field strength B_c beyond which no circular photon orbits about the z-axis can exist in the Ernst spacetime. The two physical solutions of the cubic equation for $B < B_c$ are denoted as r_1 and r_2 (with $r_2 < r_1$), the latter of which closely resembles the Schwarzschild photon sphere at $r = 3M$ for weak magnetic fields, while the former has no analogy in the Schwarzschild spacetime. Further exploring the stability of these orbits, our results show that r_2 is always unstable to radial perturbations, similar to the Schwarzschild photon sphere. However, r_1 is always stable with respect to r, unlike Schwarzschild spacetime, which only admits unstable circular lightlike orbits. Both r_1 and r_2 are stable with respect to θ-perturbations. Since r_3 (when real) is always negative hence its stability is not discussed. Restricting to a meridional plane ($\dot{\phi} = 0$), the spacetime becomes conformal to the Schwarzschild spacetime; hence, the lightlike geodesics are the same in the meridional planes of both the spacetimes. This allows us to identify unstable photon orbits at $r = 3M$ around the Schwarzschild-Melvin black hole.

Following this, we explore spherical lightlike geodesics in the Ernst spacetime to create an analogy with the axisymmetric Kerr spacetime. We prove that the circular lightlike geodesics about the z-axis in the equatorial plane and those in the meridional plane are the only spherical lightlike geodesics. Solving for the spherical lightlike geodesic conditions, we find an expression for the ratio of the constants E and L. However, the dependence of this expression on the variable θ leads to our conclusion that, except for the known circular geodesics, spherical lightlike geodesics do not exist in the Ernst spacetime.

Afterwards, we provide the exact bending angle formula for the meridional plane, which coincides with that obtained in the Schwarzschild spacetime. However, the notion of a bending angle in the equatorial plane is not valid, as we find that a light ray that goes through a minimum radius r_m with a non-zero angular momentum L cannot escape to infinity.

Next, we obtain expressions for the angular diameters of the shadow for the meridional and equatorial planes, denoted, respectively, as α and β. The former coincides with the Schwarzschild formula for black hole shadow, while the conserved quantity

$\tilde{L}$ plays the role of angular momentum L in Schwarzschild spacetime. We show that $\beta > \alpha$, leading to an oblate geometry of the shadow in the Ernst spacetime.

Furthermore, we explore the case of photon rings in the Ernst spacetime. We obtain an expression for the gap parameter Δ_n , which is the relative separation between two consecutive photon rings, where n is the order of the rings. Plotting this parameter for $n = 2$ for different values of the magnetic field strength B we obtain the characteristic range of the gap parameter for an observer along the black hole's axis. We identify the value of B beyond which the gap parameter Δ_2 values can help distinguish the Schwarzschild-Melvin black hole from the Schwarzschild case.

In conclusion, this work provides a detailed understanding of how magnetic fields influence photon dynamics near black holes, offering new insights into the behaviour of light in strong-field gravity and its observational consequences.

تحقیق کا خلاصہ

بلیک ہولز(black-holes) کے گرد جیوڈیسکس(geodesics) کا مطالعہ گریویٹیشنل لینسنگ(Gravitational-Lensing)، شیڈو(shadow) کی تشکیل، اور کمپیکٹ(compact) اشیاء کے قریب فلکی طبیعی عمل کو سمجھنے میں بنیادی حیثیت رکھتا ہے۔ اس کام میں، ہم ارنسٹ اسپیس ٹائم(Ernst-spacetime) جسے شوارز شلڈ-میلوِن(Schwarzschild-Melvin) بلیک ہول بھی کہا جاتا ہے۔ میں لائٹ لائک(lightlike) جیوڈیسک کی تحقیقات کرتے ہیں، جو ایک بیرونی یکساں مقناطیسی فیلڈ(field) میں ڈوبے ہوئے Schwarzschild بلیک ہول کو بیان کرتا ہے۔ اس مقناطیسی فیلڈ B کی موجودگی روشنی کی شعاعوں کے راستے کو تبدیل کرتی ہے، جس کے نتیجے میں شوارز شلڈ کیس کے مقابلے فوٹون جیوڈیسک کی ساخت میں نمایاں تبدیلیاں آتی ہیں۔

ہم ارنسٹ اسپیس ٹائم میں لائٹ لائک جیوڈیسکس کی وضاحت کرتے ہیں اور استوائی(equatorial) اور میریڈیونل(meridional) پلین میں دائرہ نما(circular) لائٹ لائک جیوڈیسکس کے لیے شرائط حاصل کرتے ہیں۔ ہملٹونیائی(Hamiltonian) فارملزم استعمال کرتے ہوئے، ہم کوارڈینیٹ(coordinate) r میں ایک تکعبی مساوات(cubic-equation) اخذ کرتے ہیں، جس کے حل دائرہ نما فوٹون مداروں کے ممکنہ رداس کا تعین کرتے ہیں۔ ہمارا تجزیہ ظاہر کرتا ہے کہ ایسے مدار صرف استوائی پلین میں ممکن ہیں، جبکہ ہم ایک انتقادی(critical) مقناطیسی فیلڈ B_C کی شناخت کرتے ہیں جس سے آگے ارنسٹ اسپیس ٹائم میں z محور کے گرد کوئی دائرہ نما فوٹون مدار موجود نہیں رہتا۔ مساوات کے دو حقیقی حل r_1 اور r_2 کہلاتے ہیں (جہاں $r_2 < r_1$)۔ r_2 کمزور مقناطیسی فیلڈ کے لیے شوارز شلڈ فوٹون سفیئر(photon-sphere) سے مشابہ ہے، جبکہ r_1 کی کوئی مثال شوارز شلڈ اسپیس ٹائم میں موجود نہیں۔ مزید برآں، مداروں کے استحکام(stability) کے مطالعے سے پتا چلتا ہے کہ r_2 ہمیشہ ریڈیل(radial) خلل کے لیے غیر مستحکم رہتا ہے، جبکہ r_1 ہمیشہ مستحکم رہتا ہے، جو شوارز شلڈ کیس سے مختلف ہے۔ دونوں مدار θ کی سمت میں استحکام رکھتے ہیں۔ تیسرا حل r_3 (جب حقیقی ہو) ہمیشہ منفی ہوتا ہے، اس لیے ہم اس کی مزید وضاحت نہیں کرتے۔ میریڈیونل پلین ($\dot{\phi} = 0$) تک محدود رہتے ہوئے، اسپیس ٹائم شوارز شلڈ اسپیس ٹائم کے کنفارمل(conformal) ہوتا ہے، لہٰذا دونوں اسپیس ٹائمز میں لائٹ لائک جیوڈیسکس ایک جیسے رہتے ہیں۔ اس سے ہمیں شوارز شلڈ–میلوِن بلیک ہول کے ارد گرد $r = 3M$ پر غیر مستحکم فوٹون مداروں کی شناخت کرنے کا موقع ملتا ہے۔

اس کے بعد، ہم ارنسٹ اسپیس ٹائم میں کروی(spherical) لائٹ لائک جیوڈیسکس کا مطالعہ کرتے ہیں تاکہ اس کا موازنہ غیر متقارن کیر اسپیس(Kerr-spacetime) ٹائم سے کیا جا سکے۔ ہم یہ ثابت کرتے ہیں کہ استوائی پلین میں z محور کے گرد دائرہ نما لائٹ لائک جیوڈیسکس اور میریڈیونل پلین میں موجود مدار ہی واحد کروی لائٹ لائک جیوڈیسکس ہیں۔ کروی لائٹ لائک جیوڈیسکس کی شرائط حل کرتے ہوئے، ہم E اور L کے تناسب کا اخذ کرتے ہیں۔ تاہم اس کا θ پر انحصار ہمیں اس نتیجے تک پہنچاتا ہے کہ معلوم شدہ دائرہ نما مداروں کے علاوہ ارنسٹ اسپیس ٹائم میں کوئی کروی لائٹ لائک جیوڈیسکس موجود نہیں۔

بعد ازاں، ہم میریڈیونل پلین کے لیے زاویائی انحراف(bending-angle) کا فارمولا فراہم کرتے ہیں، جو بالکل شوارز شلڈ اسپیس ٹائم سے مطابقت رکھتا ہے۔ تاہم استوائی پلین میں زاویائی انحراف کا تصور درست نہیں، کیونکہ غیر صفر زاویائی مومینٹم(angular-momentum) L کے ساتھ کم از کم رداس r_m سے گزرنے والی شعاع لامحدود(infinity) تک نہیں پہنچ سکتی۔

اگلے مرحلے میں، ہم سائے کے زاویائی قطر(angular-radius) کے فارمولا اخذ کرتے ہیں، جنہیں α (میریڈیونل) اور β (استوائی) کہتے ہیں۔ α شوارز شلڈ فارمولا سے مطابقت رکھتا ہے، جبکہ ایک محفوظ شدہ مقدار(conserved-quantity) $\tilde{L}$ شوارز شلڈ اسپیس ٹائم میں L کے کردار کو ادا کرتی ہے۔ ہم دکھاتے ہیں کہ β ہمیشہ α سے بڑا ہوتا ہے، جس سے ارنسٹ اسپیس ٹائم میں سائے کی شکل ابلیٹ(oblate) ہو جاتی ہے۔

مزید برآں، ہم ارنسٹ اسپیس ٹائم میں فوٹون رنگز(photon-rings) کا مطالعہ کرتے ہیں۔ ہم گیپ پیرامیٹر(gap-parameter) Δ_n کا فارمولا اخذ کرتے ہیں، جو دو لگاتار فوٹون رنگز کے درمیان فاصلہ ہے، جہاں n رنگ کے آرڈر کا تعین کرتا ہے۔ $n = 2$ کے لیے مختلف B قدروں پر اس پیرامیٹر کی نقشہ سازی کر کے، ہم اس کا خاص دائرہ کار حاصل کرتے ہیں۔ ہم اس انتقادی B کی نشاندہی کرتے ہیں جس سے آگے Δ_2 کی قدریں شوارز شلڈ–میلوِن بلیک ہول کو شوارز شلڈ کیس سے ممتاز کر سکتی ہیں۔

یہ کام اس بات کی مفصل تفہیم فراہم کرتا ہے کہ کس طرح مقناطیسی فیلڈ بلیک ہولز کے قریب فوٹون ڈائنامکس(dynamics) کو متاثر کرتے ہیں، اور یہ روشنی کے رویے اور مشاہداتی مظاہر کے حوالے سے نئے نتائج پیش کرتا ہے۔

Chapter 1

Introduction

1.1 Background and Motivation

The motion of light around black holes has been a subject of significant interest in general relativity and astrophysics [Perlick (2004); Claudel et al. (2001); Cunha and Herdeiro (2018)]. The study of photon orbits is crucial for understanding gravitational lensing, black hole shadows, photon rings and light deflection near compact objects.

While many studies have focused on geodesic motion in vacuum solutions, real astrophysical black holes are often surrounded by magnetic fields, particularly in active galactic nuclei (AGNs), accretion disks and magnetars [Duncan and Thompson (1992)]. Such magnetic fields interact with photon trajectories in nontrivial ways, modifying their trajectories and leading to new effects in light propagation. One of the simplest models that incorporates an external magnetic field is the Ernst spacetime, also known as the Schwarzschild-Melvin black hole, which describes a Schwarzschild black hole immersed in a uniform magnetic field [Ernst (1976)].

The magnetic field modifies this spacetime by introducing a factor Λ, which alters the effective potential and changes the lightlike and timelike geodesics [Konoplya (2003)]. Not only do the number and stability of circular photon orbits differ significantly from the Schwarzschild case, but effects such as spherical orbits, bending angle and shadow structure are different from the other known spacetimes, leading to new physical insights into how black hole environments behave under strong magnetic fields.

1.2 Research Objectives

In this work, we aim to:

1. Discuss lightlike and timelike geodesics in the Ernst spacetime by solving the geodesic equations.

2. Analyze the number and stability of circular photon and timelike orbits and identify a critical value of magnetic field strength B that governs these geodesics.

3. Explore motion in a meridional plane and the conformal relation with the Schwarzschild solution.

4. Investigate the absence of spherical orbits oscillating in θ, unlike other axisymmetric spacetimes like the Kerr solution.

5. Derive formulas for angular deflection in the meridional and equatorial planes.

6. Explore the analytical properties of the black hole shadow radius.

7. Extend our understanding of photon rings to the Ernst spacetime and evaluate the gap parameter expression.

By achieving these objectives, we provide a deeper understanding of how strong magnetic fields influence photon dynamics near black holes. These results could have important astrophysical implications for interpreting black hole imaging and lensing in highly magnetized environments.

1.3 Structure of the Thesis

This thesis is divided into 8 chapters, as follows:

- **Chapter 2** presents the Schwarzschild-Melvin (Ernst) metric, discussing its key properties and differences from the Schwarzschild solution.
- **Chapter 3** discusses the geodesics of lightlike and timelike objects.
- **Chapter 4** details the properties of the circular lightlike geodesics.
- **Chapter 5** explores the exact angular deflection formula in the meridional plane against the minimum radius value r_m.
- **Chapter 6** discusses the angular shadow properties of the Schwarzschild-Melvin black hole.
- **Chapter 7** presents photon rings in the Ernst spacetime and the effect of the magnetic field on the gap parameter Δ_n.
- **Chapter 8** concludes with a discussion of the implications of our findings and outlines future research directions.

Chapter 2

Ernst solution

2.1 Introduction

The Schwarzschild-Melvin metric, also known as the Ernst solution [Ernst (1976)], describes a Schwarzschild black hole immersed in an external, uniform magnetic field. This solution arises from the Einstein-Maxwell equations, which govern the interaction between gravity and electromagnetism in general relativity [Stephani et al. (2003); Griffiths and Podolský (2009)]. It represents an electrovacuum solution, meaning that while the spacetime is sourced by an electromagnetic field, there are no charged matter sources present. This metric generalizes two well-known spacetimes: the standard Schwarzschild metric when the magnetic field strength $B = 0$ and the Bonnor-Melvin magnetic universe when mass $M = 0$ [Bonnor (1954); Melvin (1964)].

A key feature of the Ernst solution is that the external magnetic field alters the global properties of spacetime, leading to non-asymptotic flatness.

2.2 Spacetime

The Einstein-Maxwell equations describe the coupling between the gravitational field (metric $g_{\mu\nu}$) and the electromagnetic field (described by the electromagnetic field tensor $F_{\mu\nu}$). The Ernst solution is obtained by solving these equations under the assumption of a static and axisymmetric spacetime with an external, uniform magnetic field.

The metric is given by

$$ds^2 = -\Lambda^2 \left(1 - \frac{2M}{r}\right) dt^2 + \frac{\Lambda^2}{\left(1 - \frac{2M}{r}\right)} dr^2 + r^2 \Lambda^2 d\theta^2 + \frac{r^2 \sin^2\theta}{\Lambda^2} d\phi^2, \tag{2.1}$$

where the factor Λ is defined as

$$\Lambda = 1 + \frac{1}{4} r^2 B^2 \sin^2\theta. \tag{2.2}$$

Note that throughout this thesis, we will use the principal ($G = c = 1$) units.

It is an important observation that Λ does not affect the radius of the event horizon of the black hole, and like the Schwarzschild case, the Schwarzschild-Melvin black hole also has an event horizon at $r = 2M$.

2.3 The Bonnor-Melvin Magnetic Universe as a Special Case

If we set $M = 0$, the Ernst metric reduces to the Bonnor-Melvin magnetic universe, which is a self-gravitating magnetic field configuration in general relativity [Bonnor (1954); Melvin (1964)]. The Bonnor-Melvin solution is given by

$$ds^2 = -\Lambda^2 dt^2 + \Lambda^2 dr^2 + r^2\Lambda^2 d\theta^2 + \frac{r^2 \sin^2\theta}{\Lambda^2} d\phi^2. \tag{2.3}$$

Unlike the Schwarzschild spacetime, this is not a black hole solution, but rather a uniformly magnetized universe. The gravitational attraction from the energy density of the magnetic field balances the field's tendency to disperse, leading to a stable structure. This case is interesting because it represents a highly curved, purely magnetized spacetime with no event horizon, highlighting how magnetic fields alone can create gravitational effects.

2.4 Key Properties of the Ernst Spacetime

2.4.1 Staticity

Ernst spacetime is static, meaning that it possesses a global timelike Killing vector field ∂_t that is hypersurface orthogonal, ensuring the absence of any time dependence in the metric. This means that energy E is a conserved quantity along a geodesic.

2.4.2 Axisymmetry

Ernst spacetime admits a rotational symmetry along the ϕ direction and for a coordinate system with the external magnetic field along the z-direction, the z-component of the angular momentum L stays conserved.

2.4.3 Non-Asymptotic Flatness

Unlike the Schwarzschild metric, the Ernst solution is not asymptotically flat. In Schwarzschild spacetime, at large distances from the black hole, the metric approaches Minkowski space. However, in the Ernst spacetime, the external magnetic field persists at arbitrarily large distances, meaning the spacetime does not resemble flat space even at infinity. At infinity, the Ernst spacetime reduces to the Melvin-Bonnor solution as given by Eq. (2.3).

This has significant implications:

- No conventional event horizon behaviour at infinity: unlike Schwarzschild, the light cones do not asymptotically flatten out.
- Light deflection is different: The external field alters photon trajectories, even for distant observers.
- Black hole shadows geometry and gravitational lensing effects are modified.

2.4.4 Effect of B on Geodesics and the Horizon

The magnetic field B introduces additional gravitational effects that modify the photon sphere and lead to additional constraints on circular orbits. The location of the event horizon remains at $r = 2M$, but the properties of the Schwarzschild photon sphere and the effective potential are no longer valid.

2.5 Conclusion

The Ernst solution provides a natural setting for studying magnetized black holes, offering insights into the behavior of geodesics, photon motion and light deflection in strong-field gravity. The non-asymptotic flatness and the presence of an external magnetic field significantly alter standard geodesic structures, making this spacetime an important model for astrophysical applications such as black hole imaging and gravitational lensing in highly magnetized environments.

This discussion sets the stage for the detailed study of lightlike geodesics in the next chapter, where we derive the conditions for circular photon orbits and analyze their stability.

Chapter 3

Geodesic Motion

3.1 Introduction

The study of geodesics in Ernst spacetime is crucial for understanding how an external uniform magnetic field modifies light propagation near a black hole. Unlike the standard Schwarzschild case, where photon trajectories are governed by the vacuum Einstein equations, the presence of a magnetic field introduces an additional parameter that alters the geodesic motion.

In this chapter, we describe the dynamics of lightlike and timelike geodesics using the Hamiltonian formalism. Instead of solving the geodesic equation directly, we formulate the problem in terms of Hamilton's equations, which offer a systematic approach to deriving the constants of motion and understanding the conditions for geodesic motion.

3.2 Lagrangian Formalism

For a spacetime given by the metric $g_{\mu\nu}$, the Lagrangian is provided by

$$\mathcal{L} = \frac{1}{2} g_{\mu\nu} \dot{x}^\mu \dot{x}^\nu, \tag{3.1}$$

where the overdot indicates differentiation with respect to an affine parameter. The following Lagrangian governs the geodesics in the Ernst spacetime,

$$\mathcal{L} = \frac{1}{2}\left[-\Lambda^2 \left(1 - \frac{2M}{r}\right) \dot{t}^2 + \frac{\Lambda^2}{\left(1 - \frac{2M}{r}\right)} \dot{r}^2 + r^2 \Lambda^2 \dot{\theta}^2 + \frac{r^2 \sin^2\theta}{\Lambda^2} \dot{\phi}^2 \right] = \frac{1}{2}\epsilon, \tag{3.2}$$

where the constant ϵ takes up values of 0 and -1 for lightlike and timelike geodesics, respectively.

As discussed in Sec. 2.4, the Ernst spacetime admits two global symmetries: staticity and axisymmetry. Thus, it admits two Killing vectors associated with conserved quantities: Energy E due to time translation symmetry: $p_t = -E$

$$-\frac{\partial \mathcal{L}}{\partial \dot{t}} = E = \Lambda^2 \left(1 - \frac{2M}{r}\right) \dot{t}, \tag{3.3}$$

and angular momentum L due to axial symmetry: $p_\phi = L$

$$\frac{\partial \mathcal{L}}{\partial \dot{\phi}} = L = \frac{r^2 \sin^2\theta}{\Lambda^2} \dot{\phi}. \tag{3.4}$$

This allows us to re-express the Lagrangian as

$$\mathcal{L} = \frac{1}{2}\left[-\frac{1}{\Lambda^2(1-\frac{2M}{r})}E^2 + \frac{\Lambda^2}{r^2\sin^2\theta}L^2 + \frac{\Lambda^2}{(1-\frac{2M}{r})}\dot{r}^2 + r^2\Lambda^2\dot{\theta}^2\right] = \frac{1}{2}\epsilon. \tag{3.5}$$

Multiplying by $r^2\sin^2\theta/\Lambda^2$ and readjusting the terms

$$\frac{r^2\sin^2\theta}{\Lambda^4(1-\frac{2M}{r})}E^2 + \frac{r^2\sin^2\theta}{\Lambda^2}\epsilon = L^2 + \frac{r^2\sin^2\theta}{\left(1-\frac{2M}{r}\right)}\dot{r}^2 + r^4\sin^2\theta\,\dot{\theta}^2.$$

Note that in the interval $2M < r < \infty$, the right-hand side of the equation is strictly positive for $L \neq 0$. This means that the left-hand side is also positive for this case. Eq. (3.4) tells us that for $L \neq 0$, $\sin\theta \neq 0$ meaning that we are away from the pole. However, for $B \neq 0$, the left-hand side of the equation approaches 0 for $r \to \infty$. This leads to a contradiction. The only resolution is that for a non-zero magnetic field strength $B \neq 0$, any geodesic with a non-zero z-component of angular momentum $L \neq 0$ cannot escape to infinity. This extends the results of Dhurandhar and Sharma [Dhurandhar and Sharma (1983)] who showed that lightlike geodesics in the equatorial plane with $L \neq 0$ cannot reach infinity.

3.3 Hamilton's Formalism of Geodesics

We can pass from the Lagrangian to the Hamiltonian formalism using the relation

$$\mathcal{H}(x,p) = \dot{x}^\mu p_\mu - \mathcal{L}(\dot{x},x). \tag{3.6}$$

Note that

$$\mathcal{H}(x,p) = \mathcal{L}(\dot{x},x) = \frac{1}{2}\epsilon, \tag{3.7}$$

meaning that the Hamiltonian is given by the same quantity as the Lagrangian, except that it is expressed in terms of canonical momenta instead of velocities. Thus, the Hamiltonian can be expressed as

$$\mathcal{H} = \frac{1}{2}\left[-\frac{E^2}{\Lambda^2\left(1-\frac{2M}{r}\right)} + \frac{L^2\Lambda^2}{r^2\sin^2\theta} + \frac{p_r^2\left(1-\frac{2M}{r}\right)}{\Lambda^2} + \frac{p_\theta^2}{r^2\Lambda^2}\right]. \tag{3.8}$$

Applying Hamilton's first equation

$$\dot{q}_\mu = \frac{\partial\mathcal{H}}{\partial p_\mu}, \tag{3.9}$$

we get

$$\dot{t} = \frac{E}{\Lambda^2\left(1-\frac{2M}{r}\right)}, \tag{3.10}$$

$$\dot{\phi} = \frac{L\Lambda^2}{r^2\sin^2\theta}, \tag{3.11}$$

$$\dot{r} = \frac{p_r\left(1 - \frac{2M}{r}\right)}{\Lambda^2}, \tag{3.12}$$

$$\dot{\theta} = \frac{p_\theta}{r^2\Lambda^2}. \tag{3.13}$$

Similarly, applying Hamilton's second equation

$$\dot{p}_\mu = -\frac{\partial \mathcal{H}}{\partial q_\mu}, \tag{3.14}$$

which yields

$$\dot{p}_r = \left[\frac{2\Lambda^2 M}{(r-2M)^2} - \frac{\Lambda r^2 B^2 \sin^2\theta}{r-2M}\right]\dot{r}^2 - \left[2\Lambda^2 r + \Lambda r^3 B^2 \sin^2\theta\right]\dot{\theta}^2,$$

$$\dot{p}_\theta = -\left[\frac{1}{\left(1 - \frac{2M}{r}\right)}\dot{r}^2 + r^2\dot{\theta}^2\right]\Lambda r^2 B^2 \sin\theta\cos\theta,$$

$$\dot{p}_t = \dot{p}_\phi = 0.$$

Since p_t and p_ϕ are conserved, we focus on solving for the motion in the radial and angular directions.

3.4 Circular Lightlike Geodesics about the z-axis

For a circular photon orbit about the z-axis, we require that both the radial velocity and acceleration vanish

$$\dot{r} = 0, \quad \ddot{r} = 0.$$

This implies that

$$p_r = 0, \quad \dot{p}_r = 0.$$

Similarly, we want both the angular velocity and acceleration vanish

$$\dot{\theta} = 0, \quad \ddot{\theta} = 0,$$

implying that

$$p_\theta = 0, \quad \dot{p}_\theta = 0.$$

From these conditions, the Hamiltonian simplifies to

$$\mathcal{H} = -\frac{E^2}{\Lambda^2\left(1 - \frac{2M}{r}\right)} + \frac{L^2\Lambda^2}{r^2\sin^2\theta}, \tag{3.15}$$

Since we are dealing with lightlike geodesics, $\mathcal{H} = 0$. This defines a potential

$$V = -\frac{E^2}{\Lambda^2\left(1 - \frac{2M}{r}\right)} + \frac{L^2\Lambda^2}{r^2\sin^2\theta} = 0. \tag{3.16}$$

Rearranging for L^2/E^2 gets us

$$\frac{L^2}{E^2} = \frac{r^3\sin^2\theta}{\Lambda^4(r-2M)}. \tag{3.17}$$

3.4.1 Deriving the Cubic Equation for r

The condition $\ddot{r} = 0$ for circular orbits requires $\partial V/\partial r = 0$, leading to

$$E^2\left[\frac{r^2B^2\sin^2\theta}{\Lambda^3(r-2M)} + \frac{2M}{\Lambda^2(r-2M)^2}\right] + L^2\left[\frac{\Lambda r B^2\sin^2\theta}{r^2\sin^2\theta} - \frac{2\Lambda^2}{r^3\sin^2\theta}\right] = 0. \tag{3.18}$$

Again, solving for L^2/E^2 gets us

$$\frac{L^2}{E^2} = \frac{r^3\sin^2\theta[r^2B^2\sin^2\theta(r-2M)+2M\Lambda]}{\Lambda^4(r-2M)^2(2\Lambda - r^2B^2\sin^2\theta)}. \tag{3.19}$$

Using Eq. (3.17) and the equation above, we arrive at the following cubic equation:

$$\left(3B^2\sin^2\theta\right)r^3 - \left(5MB^2\sin^2\theta\right)r^2 - 4r + 12M = 0. \tag{3.20}$$

Similarly, the condition $\ddot{\theta} = 0$ demands $\partial V/\partial\theta = 0$ that gets us

$$\left[E^2\frac{r^3B^2\sin\theta}{\Lambda^3(r-2M)} - L^2\left(\frac{2\Lambda^2}{r^2\sin^3\theta} - \frac{\Lambda B^2}{\sin\theta}\right)\right]\cos\theta = 0, \tag{3.21}$$

where $\cos\theta = 0 \to \theta = \pi/2$ is the trivial solution. We can solve for the expression inside the parentheses to see if that gives us a zero. Solving for L^2/E^2 gets us

$$\frac{L^2}{E^2} = \frac{r^5B^2\sin^4\theta}{\Lambda^4(r-2M)(2\Lambda - r^2B^2\sin^2\theta)}. \tag{3.22}$$

Using Eq. (3.17) and the equation above we arrive at

$$rB\sin\theta = \frac{2}{\sqrt{3}}. \tag{3.23}$$

If this solution satisfies the cubic equation (3.20), it would provide us with circular light-like geodesics around the z-axis outside of the equatorial plane. Putting $r = \frac{2}{\sqrt{3}B\sin\theta}$ in Eq. (3.20)

$$\begin{gathered}
\left(3B^2\sin^2\theta\right)\left(\frac{2}{\sqrt{3}B\sin\theta}\right)^3 - \left(5MB^2\sin^2\theta\right)\left(\frac{2}{\sqrt{3}B\sin\theta}\right)^2 \\
-4\left(\frac{2}{\sqrt{3}B\sin\theta}\right) + 12M = 0, \\
\frac{8}{\cancel{\sqrt{3}}B\sin\theta} - \frac{20M}{3} - \frac{8}{\cancel{\sqrt{3}}B\sin\theta} + 12M = 0, \\
\frac{16M}{3} \neq 0.
\end{gathered}$$

For a non-zero black hole mass, this equation is not zero. Therefore, the only solution to Eq. (3.21) is $\theta = \pi/2$. This implies that in Ernst spacetime, circular light-like geodesics around the z-axis exist only in the equatorial plane. Eq. (3.20), thus, reduces to

$$3B^2r^3 - 5MB^2r^2 - 4r + 12M = 0. \tag{3.24}$$

This equation determines the allowed radii for circular lightlike geodesics about the z-axis based on the strength of the magnetic field B in the equatorial plane. Esteban [Esteban (1984)] arrived at this equation for the circular lightlike geodesics in the equatorial plane of the Ernst spacetime. Dhurandhar and Sharma [Dhurandhar and Sharma (1983)] also obtained the same cubic equation valid for $B \to 2B$.

3.4.2 Solving for the Radial Coordinate

The cubic equation (3.24) can be presented in the form

$$ax^3 + bx^2 + cx + d = 0,$$

where

$$a = 3B^2, \quad b = -5MB^2, \quad c = 4, \quad d = 12M.$$

Solving this equation in closed form is possible using Cardano's method. The three roots are given by:

$$r_1 = \frac{(X+Y)^{\frac{1}{3}}}{9B^2} - \frac{Z}{9B^2\,(X+Y)^{\frac{1}{3}}} + \frac{5M}{9} \tag{3.25}$$

$$r_2 = \frac{-(1+i\sqrt{3})\,(X+Y)^{\frac{1}{3}}}{18B^2} + \frac{(1-i\sqrt{3})Z}{18B^2\,(X+Y)^{\frac{1}{3}}} + \frac{5M}{9} \tag{3.26}$$

$$r_3 = \frac{-(1-i\sqrt{3})\,(X+Y)^{\frac{1}{3}}}{18B^2} + \frac{(1+i\sqrt{3})Z}{18B^2\,(X+Y)^{\frac{1}{3}}} + \frac{5M}{9} \tag{3.27}$$

Where

$$X = 125B^6M^3 - 1188B^4M, \tag{3.28}$$

$$Y = 18\sqrt{3}\sqrt{-375B^{10}M^4 + 1352B^8M^2 - 48B^6}, \tag{3.29}$$

$$Z = -25B^4M^2 - 36B^2. \tag{3.30}$$

We have obtained three solutions of the cubic equation: r_1, r_2 and r_3. These solutions represent the circular lightlike orbits about the z-axis of the Ernst spacetime. For static and symmetric spacetimes like the Schwarzschild, we can reduce our equations to the equatorial plane and examine the lightlike geodesics. The solutions thus obtained are valid for any arbitrary θ value. However, the Ernst metric is not spherically symmetric but rather axisymmetric. Therefore, when we call them "circular lightlike geodesics," we specifically speak of circular geodesics about the z-axis.
We will later show in Chapter 4 that for a sub-critical magnetic field strength B_c, $r_3 < 0$ while $r_2 < r_1$. We will discuss the properties of these solutions in detail in Chapter 4.

3.5 Conformal Relationship with Schwarzschild Spacetime

Junior *et al.* [Lima Junior et al. (2022)] identified that when reduced to a meridional plane $\dot{\phi} = 0$, the Ernst spacetime is conformal to the Schwarzschild spacetime restricted to the meridional plane.
For the meridional plane ($\dot{\phi} = 0$) and null geodesics the Lagrangian (3.2) reduces to

$$\mathcal{L} = \frac{1}{2}\left[-\Lambda^2 \left(1 - \frac{2M}{r}\right) \dot{t}^2 + \frac{\Lambda^2}{\left(1 - \frac{2M}{r}\right)} \dot{r}^2 + r^2 \Lambda^2 \dot{\theta}^2 \right] = 0, \tag{3.31}$$

$$\mathcal{L} = \frac{1}{2}\Lambda^2\left[-\left(1 - \frac{2M}{r}\right) \dot{t}^2 + \frac{1}{\left(1 - \frac{2M}{r}\right)} \dot{r}^2 + r^2 \dot{\theta}^2 \right] = 0 \tag{3.32}$$

This is the conformal transformation of the Schwarzschild metric reduced to the meridional plane with Λ^2 the conformal factor. This means that the trajectories of lightlike geodesics in the meridional plane of the Ernst spacetime will be the same as those in the meridional plane of the Schwarzschild spacetime.

The meridional plane is the union of two half-planes ϕ_o and $\phi_o + \pi$ where θ is a double-valued function. On one circle around the center, its values range from 0 to π, while on the other, it goes from π to 0. Therefore, in the meridional plane, we have the liberty to redefine

$$\theta \to \tilde{\phi}, \tag{3.33}$$

such that $\tilde{\phi}$ takes the values from 0 to 2π. In this case the Ernst metric can be rewritten as

$$ds^2 = \tilde{\Lambda}^2\left[-\left(1 - \frac{2M}{r}\right) dt^2 + \frac{1}{\left(1 - \frac{2M}{r}\right)} dr^2 + r^2 d\tilde{\phi}^2 \right] \tag{3.34}$$

where we have the following conformal factor

$$\tilde{\Lambda}^2 = 1 + \frac{1}{4} r^2 B^2 \cos^2 \tilde{\phi}. \tag{3.35}$$

For the lightlike geodesics, we can redfine the Lagrangian as

$$\tilde{\mathcal{L}} = \frac{1}{2}\Lambda^2\left[-\left(1 - \frac{2M}{r}\right) \dot{t}^2 + \frac{1}{\left(1 - \frac{2M}{r}\right)} \dot{r}^2 + r^2 \dot{\tilde{\phi}}^2 \right] = 0, \tag{3.36}$$

providing us with the conserved quantities

$$-\frac{\partial \mathcal{L}}{\partial \dot{t}} = E = \left(1 - \frac{2M}{r}\right) \dot{t}, \tag{3.37}$$

$$\frac{\partial \mathcal{L}}{\partial \dot{\tilde{\phi}}} = \tilde{L} = r^2 \dot{\tilde{\phi}}. \tag{3.38}$$

Here, $\tilde{L}$ can be interpreted as an angular momentum that emerges because the $\tilde{\phi}$ coordinate becomes cyclic. Thus, now we have 3 conserved quantities: $E, \tilde{L}$ and $\mathcal{L}$ in a $(2+1)$-dimensional system in the meridional plane. This means that the lightlike geodesic equations are fully integrable.

3.5.1 Photon Orbits

We know that there exists a photon sphere in the Schwarzschild spacetime at $r = 3M$. This means that at every point on this sphere, there exists an infinite number of circular lightlike geodesics. Since our spacetime becomes conformal to the Schwarzschild spacetime in the meridional plane, we can expect photon orbits in the meridional planes of the Ernst spacetime too. We now evaluate the presence of bound photon orbits in the meridional plane of the Ernst spacetime.

Solving the Euler-Lagrange equation for the coordinate r

$$\frac{d}{d\tilde{\lambda}}\left[\frac{1}{\left(1-\frac{2M}{r}\right)}\dot{r}\right] = \frac{1}{2}\left[-\left(\frac{2M}{r^2}\right)\dot{t}^2 - \frac{1}{\left(1-\frac{2M}{r}\right)}\left(\frac{2M}{r^2}\right)\dot{r}^2 + 2r\dot{\hat{\theta}}^2\right],$$
$$-\frac{1}{\left(1-\frac{2M}{r}\right)^2}\left(\frac{2M}{r^2}\right)\dot{r}^2 + \frac{1}{\left(1-\frac{2M}{r}\right)}\ddot{r} =$$
$$\frac{1}{2}\left[-\left(\frac{2M}{r^2}\right)\dot{t}^2 - \frac{1}{\left(1-\frac{2M}{r}\right)}\left(\frac{2M}{r^2}\right)\dot{r}^2 + 2r\dot{\tilde{\phi}}^2\right].$$

For a circular orbit in the meridional plane, we have the conditions

$$\dot{r} = 0, \quad \ddot{r} = 0,$$
$$\dot{\tilde{\phi}} = 0, \quad \ddot{\tilde{\phi}} = 0.$$

Using these conditions and Eqs. (3.37) and (3.38) in the equation above and solving get us

$$\frac{\tilde{L}^2}{E^2} = \frac{rM}{\left(1-\frac{2M}{r}\right)^2}. \tag{3.39}$$

Using the same conditions in the Lagrangian gets us

$$\frac{\tilde{L}^2}{E^2} = \frac{r^2}{\left(1-\frac{2M}{r}\right)}. \tag{3.40}$$

Comparing Eqs. (3.39) and (3.40), we get

$$r = 3M. \tag{3.41}$$

This means that much like the Schwarzschild case, we should have a circular orbit in Ernst spacetime at $r = 3M$.

Thus, there exists a circular lightlike geodesic in every meridional plane at $r = 3M$ [Lima Junior et al. (2022)]. However, it must be noted that "circular" geodesics refer to the coordinate picture; however, since the Ernst spacetime is axisymmetric and not spherically symmetric, these geodesics are elongated. These orbits at $t = cte.$ span the 2-surface of the Schwarzschild-Melvin black hole geometry

$$ds^2\Big|_{t=cte.,r=3M} = 9M^2\left[\left(1+\frac{9M^2}{4}B^2\sin^2\theta\right)^2 d\theta^2 + \frac{\sin^2\theta}{\left(1+\frac{9M^2}{4}B^2\sin^2\theta\right)^2}d\phi^2\right]. \tag{3.42}$$

The intrinsic geometry of the spacetime leads to an elongated trajectory resulting in non-circular orbits.

3.6 Spherical Lightlike Geodesics

In general relativity, spherical lightlike geodesics are trajectories of photons that maintain a constant radius value r. While the circular geodesics found in Sec. 3.4 are also spherical geodesics; spherical geodesics, in general, can oscillate in the θ direction too. In this section, we explore whether we can have any other spherical geodesics. Recall that the Kerr spacetime [Kerr (1963)] is another axisymmetric solution of the Einstein Field Equations, and it admits spherical lightlike geodesics that oscillate between two extremal values of θ [Teo (2003)]. Therefore, it is worthwhile to investigate whether such geodesics exist in the Ernst spacetime.

We take the Lagrangian from Eq. (3.2) for lightlike geodesics ($\epsilon = 0$) and solve the Euler-Lagrange equation

$$\frac{d}{d\lambda}\left(\frac{\partial \mathcal{L}}{\partial \dot{q}}\right) = \frac{\partial \mathcal{L}}{\partial q}, \tag{3.43}$$

for the r coordinate

$$\begin{aligned}
&\frac{2\Lambda}{\left(1-\frac{2M}{r}\right)}\frac{\partial \Lambda}{\partial \lambda}\dot{r} - \frac{\Lambda^2}{\left(1-\frac{2M}{r}\right)^2}\left(\frac{2M}{r^2}\right)\dot{r}^2 + \frac{\Lambda^2}{\left(1-\frac{2M}{r}\right)}\ddot{r} = \\
&\quad \frac{1}{2}\Bigg[-\left\{\Lambda\left(1-\frac{2M}{r}\right)\left(rB^2\sin^2\theta\right) + \Lambda^2\left(\frac{2M}{r^2}\right)\right\}\dot{t}^2 \\
&\quad + \left\{\frac{\Lambda}{\left(1-\frac{2M}{r}\right)}\left(rB^2\sin^2\theta\right) - \frac{\Lambda^2}{\left(1-\frac{2M}{r}\right)^2}\left(\frac{2M}{r^2}\right)\right\}\dot{r}^2 \\
&\qquad + \left\{r^2\Lambda\left(rB^2\sin^2\theta\right) + 2r\Lambda^2\right\}\dot{\theta}^2 \\
&\qquad - \left\{\frac{r^2\sin^2\theta}{\Lambda^3}\left(rB^2\sin^2\theta\right) - \frac{2r\sin^2\theta}{\Lambda^2}\right\}\dot{\phi}^2\Bigg].
\end{aligned} \tag{3.44}$$

Spherical lightlike geodesics demand the conditions

$$\dot{r} = 0, \quad \ddot{r} = 0. \tag{3.45}$$

Eq. (3.44) thus becomes

$$\begin{aligned}
0 = \frac{1}{2}\Bigg[&-\left\{\Lambda\left(1-\frac{2M}{r}\right)\left(rB^2\sin^2\theta\right) + \Lambda^2\left(\frac{2M}{r^2}\right)\right\}\dot{t}^2 \\
&+ \left\{r^2\Lambda\left(rB^2\sin^2\theta\right) + 2r\Lambda^2\right\}\dot{\theta}^2 \\
&- \left\{\frac{r^2\sin^2\theta}{\Lambda^3}\left(rB^2\sin^2\theta\right) - \frac{2r\sin^2\theta}{\Lambda^2}\right\}\dot{\phi}^2\Bigg]
\end{aligned} \tag{3.46}$$

Using Eqs. (3.10) and (3.11) and rearranging

$$\dot{\theta}^2 = \frac{\left[\frac{rB^2\sin^2\theta}{\Lambda^3\left(1-\frac{2M}{r}\right)} + \frac{2M}{r^2\Lambda^2\left(1-\frac{2M}{r}\right)^2}\right]E^2 + \left[\frac{B^2\Lambda}{r} - \frac{2\Lambda^2}{r^3\sin^2\theta}\right]L^2}{\Lambda r^3 B^2\sin^2\theta + 2r\Lambda^2} \tag{3.47}$$

where E and L are the constants of motion that satisfy the null condition of the Hamiltonian for light:

$$\mathcal{H} = -\frac{E^2}{\Lambda^2(1-\frac{2M}{r})} + \frac{L^2\Lambda^2}{r^2\sin^2\theta} + r^2\Lambda^2\dot{\theta}^2 = 0.$$

Rearranging gets us

$$E^2 = \Lambda^4\left(1-\frac{2M}{r}\right)\left[\frac{L^2}{r^2\sin^2\theta} + r^2\dot{\theta}^2\right]. \tag{3.48}$$

Inserting this into Eq. (3.47) and solving

$$\dot{\theta}^2 = \frac{\left[\frac{rB^2\sin^2\theta}{\Lambda^3\left(1-\frac{2M}{r}\right)} + \frac{2M}{r^2\Lambda^2\left(1-\frac{2M}{r}\right)^2}\right]\frac{\Lambda^4\left(1-\frac{2M}{r}\right)}{r^2\sin^2\theta} + \frac{B^2\Lambda}{r} - \frac{2\Lambda^2}{r^3\sin^2\theta}}{\Lambda r^3B^2\sin^2\theta + 2r\Lambda^2 - \left[\frac{rB^2\sin^2\theta}{\Lambda^3\left(1-\frac{2M}{r}\right)} + \frac{2M}{r^2\Lambda^2\left(1-\frac{2M}{r}\right)^2}\right]\Lambda^4\left(1-\frac{2M}{r}\right)r^2}L^2 \tag{3.49}$$

Multiplying and dividing by $r^4\sin^2\theta$ and resolving get us a simplified expression for $\dot{\theta}^2$

$$\dot{\theta}^2 = \left[\frac{B^2(r-2M)}{r^2\Lambda(r-3M)} - \frac{1}{r^4\sin^2\theta}\right]L^2. \tag{3.50}$$

This expression provides us with the velocity in θ direction for spherical lightlike geodesics. Using this expression in Eq. (3.48) we get

$$\frac{L^2}{E^2} = \frac{r(r-3M)}{\Lambda^3B^2(r-2M)^2}. \tag{3.51}$$

Note that this equation holds true when $r = 3M$ leading to $L = 0$ which is the case of the photon orbit as discussed in Sec. 3.5.1. These are the orbits that stay at a constant radial value of $r = 3M$ and move along constant ϕ lines while passing through the poles. Hence, they qualify as spherical orbits. However, except for this case, constants L and E demand Λ be a constant as well. This case is true for the equatorial plane where we obtain the known circular lightlike orbits from Sec. 3.4.

$$B \neq 0 \implies \dot{\theta} = 0. \tag{3.52}$$

Hence, for a non-zero magnetic field strength, we cannot have spherical lightlike orbits that oscillate between two θ values, like in the case of Kerr.

3.7 Circular Timelike Geodesics about the z-axis

Now, we turn to investigating circular timelike geodesics. The procedure is the same as described in Sec. 3.4 except that now we take $\epsilon = 1$ in the Lagrangian. We consider uncharged timelike objects in the equatorial plane ($\theta = \pi/2$). The Lagrangian, thus, yields

$$-\frac{1}{\Lambda^2(1-\frac{2M}{r})}E^2 + \frac{\Lambda^2}{r^2}L^2 + \frac{\Lambda^2}{(1-\frac{2M}{r})}\dot{r}^2 = -1, \tag{3.53}$$

where Λ is now given by

$$\Lambda = 1 + \frac{1}{4} r^2 B^2. \tag{3.54}$$

Separating $\dot{r}^2$

$$\dot{r}^2 = \frac{\left(1 - \frac{2M}{r}\right)}{\Lambda^2} \left[\frac{E^2}{\Lambda^2 \left(1 - \frac{2M}{r}\right)} - \frac{\Lambda^2 L^2}{r^2} - 1 \right],$$
$$\dot{r}^2 = \frac{E^2}{\Lambda^4} - \left(1 - \frac{2M}{r}\right) \left(\frac{L^2}{r^2} + \frac{1}{\Lambda^2} \right).$$

Dividing by $\dot{\phi}^2$ we get

$$\frac{\dot{r}^2}{\dot{\phi}^2} = \frac{r^4}{L^2 \Lambda^4} \left[\frac{E^2}{\Lambda^4} - \left(1 - \frac{2M}{r}\right) \left(\frac{L^2}{r^2} + \frac{1}{\Lambda^2} \right) \right]. \tag{3.55}$$

3.7.1 Effective Potential $V_{E,L}$

We get the orbital equation

$$\frac{1}{2} \left(\frac{dr}{d\phi} \right)^2 + V_{E,L} = 0,$$

where we defined an effective potential $V_{E,L}$ given by

$$-2V_{E,L} = \frac{r^4}{L^2 \Lambda^4} \left[\frac{E^2}{\Lambda^4} - \left(1 - \frac{2M}{r}\right) \left(\frac{L^2}{r^2} + \frac{1}{\Lambda^2} \right) \right]. \tag{3.56}$$

For circular orbits about the z-axis, we have the conditions

$$\frac{dr}{d\phi} = 0, \quad \frac{d^2 r}{d\phi^2} = 0.$$

This gives us

$$V_{E,L} = 0, \quad V'_{E,L} = 0.$$

Using $V_{E,L} = 0$ gets us

$$L = \frac{r}{\Lambda} \sqrt{\frac{E^2}{\Lambda^2 \left(1 - \frac{2M}{r}\right)} - 1}. \tag{3.57}$$

A plot of $V_{E,L}$ is shown for different values of B is shown in Fig. 3.1. Note that $V_{E,L}$ for each B value has an extremum which corresponds to $V'_{E,L} = 0$. Next we take the derivative of the effective potential and set that to zero:

$$V'_{E,L} = \frac{E^2}{L^2} \left(\frac{2r}{\Lambda^4} - \frac{2r^3 B^2}{\Lambda^5} \right) - \frac{2M}{r^2} - \frac{1}{L^2} \left[\frac{2r}{\Lambda^2} - \frac{r^3 B^2}{\Lambda^3} - \frac{2M}{\Lambda^2} + \frac{2r^2 M B^2}{\Lambda^3} \right] = 0$$

Solving $V'_{E,L} = 0$ and using Equation (3.57) gets us

$$E^2 = \frac{2r - \frac{r^3 B^2}{\Lambda} - \frac{2M r^2 B^2}{\Lambda} - \frac{4M}{\Lambda^2}}{\frac{2r}{\Lambda^2} - \frac{2r^3 B^2}{\Lambda^3} - \frac{2M}{\Lambda^2 \left(1 - \frac{2M}{r}\right)}}.$$

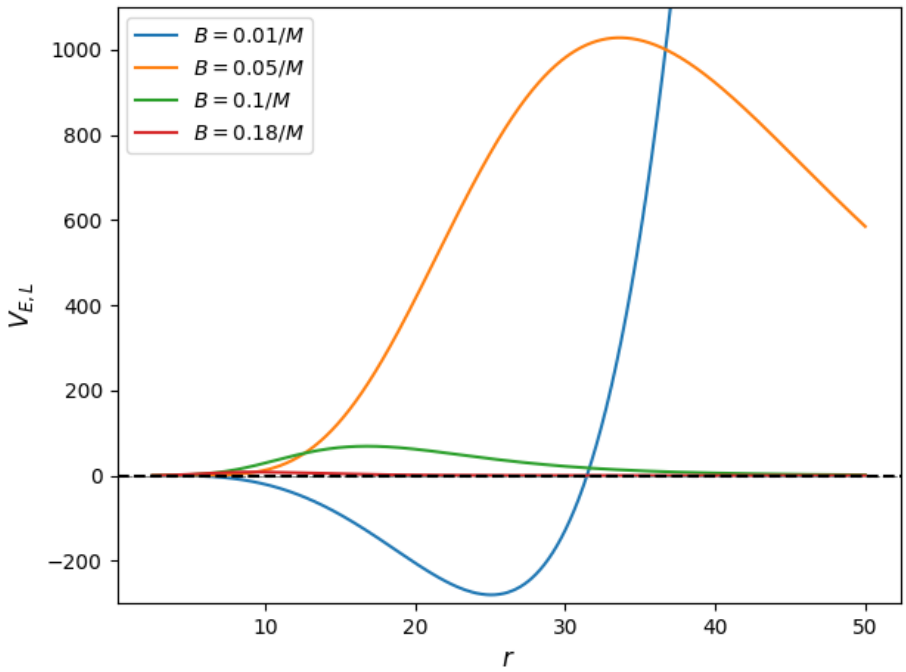

Figure 3.1: Effective potential $V_{E,L}$ from Eq. (3.56) vs. r for timelike geodesics for various B values. Here we give r in units of M and $V_{E,L}$ in units of M^2. E and L were arbitrarily chosen as 1 and $4M$.

Simplifying the expression gets us

$$E^2 = \frac{\Lambda\left(1-\frac{2M}{r}\right)\left(4Mr^2B^2-4r+8M+\frac{1}{4}B^4r^5+MB^4r^4\right)}{3B^2r^3-5MB^2r^2-4r+12M}. \tag{3.58}$$

Inserting this into Eq. (3.57) gets us

$$L^2 = \frac{r^2}{\Lambda^2}\left[\frac{4Mr^2B^2-4r+8M+\frac{1}{4}B^4r^5+MB^4r^4}{\Lambda(3B^2r^3-5MB^2r^2-4r+12M)}-1\right] \tag{3.59}$$

Note that Eqs. (3.58) and (3.59) define the conditions on the constants E and L for circular timelike geodesics in the equatorial plane of the Ernst spacetime. These expressions reduce to the known Schwarzschild results for circular timelike geodesics for $B = 0$.

$$E^2 = \frac{(r-2M)^2}{r(r-3M)}$$
$$L^2 = \frac{r^2M}{r-3M}$$

3.7.2 Allowed r range

Recognize that the denominators of Eqs. (3.58) and (3.59) contain the right-hand side of the cubic equation (3.24). Thus, $E, L \to \infty$ for the values of r that satisfy the cubic equation. Circular timelike geodesics satisfy the conditions $E^2 > 0$ and $L^2 > 0$. For

the Schwarzschild case, these conditions are satisfied for all $r > 3M$. Upon numerical analysis, for the Ernst case, we find out that for a given magnetic field strength B, E^2 and L^2 are positive for r only in the range between r_2 and r_1 where r_1 and r_2 are the radii of the circular lightlike geodesics in the equatorial plane, given by Eqs. (3.25) and (3.26), respectively. Therefore,

$$\begin{cases} E^2 > 0, L^2 > 0 & \text{if } r \in (r_2, r_1) \\ E^2 < 0, L^2 < 0 & \text{if } r \leq r_2 \text{ or } r \geq r_1 \end{cases} \tag{3.60}$$

This means that circular timelike geodesics in the equatorial plane of the Ernst spacetime can only exist between the two circular lightlike geodesics. This is not an unexpected result as r_2 and r_1 are the radii of the null geodesics and hence a timelike geodesics cannot sit in a circular geodesic for these r values.

3.7.3 Stability and ISCO Determination

Next, we obtain an expression for the second derivative of the effective potential $V_{E,L}$ and determine the radius values where the timelike circular orbits are stable:

$$\begin{aligned} \frac{\partial^2 V_{E,L}}{\partial r^2} = -\frac{256}{L^2(B^2r^2+4)^{10}}\Bigg[& L^2(B^2r^2+4)^4\Big(7B^4r^3(8M-3r)+24B^2r(3r-4M)-16\Big) \\ & + 96r\Big(M(15B^4r^4-48B^2r^2+16)(B^2r^2+4)^2 - 2r(3B^4r^4-14B^2r^2+8)(B^2r^2+4)^2 \\ & + 16e^2r(13B^4r^4-40B^2r^2+16)\Big)\Bigg]. \end{aligned} \tag{3.61}$$

The plot of $V''_{E,L}$ for various magnetic field strengths is shown in Fig. 3.2. It can be observed that for each B value, the plot of $V''_{E,L}$ intersects the x-axis only once and stays positive for the rest of the range. This point of intersection defines the Innermost Stable Circular Orbit (ISCO) for the given B value. Note that the plot does not intersect the x-axis again, indicating that we have stable timelike circular orbits for the rest of the range (r_{ISCO}, r_1). This means that the outer lightlike circular orbit radius r_1 serves as the Outer Most Stable Circular Orbit (OSCO) for timelike geodesics in the equatorial plane of the Ernst spacetime.

$$r_{\text{stable}} \in (r_{ISCO}, r_1) \tag{3.62}$$

3.8 Conclusion

In this chapter, we obtained the geodesic equations for lightlike and timelike geodesics. We identified a potential method that provides a way to determine the conditions for circular photon orbits about the z-axis. We showed that these orbits only exist in the equatorial plane. Working in the meridional plane, we obtained a conformality with the Schwarzschild spacetime that led to photon orbits at $r = 3M$. We proved that

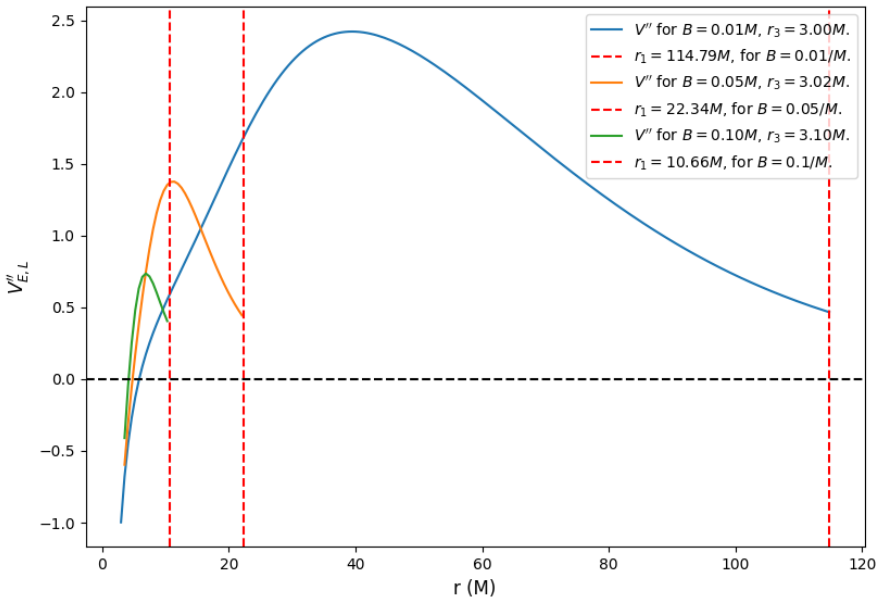

Figure 3.2: $V''_{E,L}$ vs. r for various B values. $V''_{E,L} = 0$ corresponds to the ISCO. Here we give r in units of M and $V''_{E,L}$ in units of M^2. For each r, the energy E and angular momentum L of the circular timelike orbit were used, as given by Eqs. (3.7.1) and (3.59), respectively.

circular lightlike geodesics are the only spherical lightlike geodesics that exist in the Ernst spacetime. Finally, we showed that in the Ernst spacetime between the two circular lightlike orbits, we also have circular timelike geodesics in the equatorial plane. Thus, in addition to an ISCO, we also have an OSCO in the Ernst spacetime.

This analysis sets the stage for Chapter 4, where we investigate the solutions to this equation and explore the range of B values that determine the number of circular geodesics.

Chapter 4

Properties of Circular Lightlike Geodesics

4.1 Introduction

In the previous chapter, we established the conditions for circular lightlike geodesics about the z-axis in the Ernst spacetime using the Hamiltonian formalism. By analysing the potential, we derived a constraint equation for the existence of circular lightlike orbits, which reduced to a cubic equation in the radial coordinate r. Moreover, we obtained the three solutions of the cubic equations. We also showed that circular lightlike geodesics about the z-axis cannot exist outside the equatorial plane ($\theta = \pi/2$). Therefore, now we will only consider the case of the equatorial plane.

In this chapter, we discuss the nature of these solutions that depend on the discriminant of the cubic equation, which allows us to classify the number of real roots. Specifically, we identify a critical range of B values where only one real solution exists, whereas outside this range, we obtain three distinct real roots. We analyse these solutions numerically and, following that, discuss their stability.

This transition from 3 solutions to 1 solution occurs because the discriminant of the cubic equation becomes negative, meaning that two of the solutions become complex conjugates and thus physically meaningless.

4.2 Discriminant Analysis

Eqs. (3.25) - (3.27) provide the solutions of the cubic equation (3.24). Note that r_2 and r_3 have the complex number i in them, and all three solutions have square-root terms with possible negative arguments. Therefore, the solutions need to be carefully analyzed.

To confirm the number of real roots, we use the discriminant Δ of the cubic equation

$$\Delta = -4p^3 - 27q^2, \tag{4.1}$$

where p and q are obtained from the depressed cubic form

$$ax^3 + bx^2 + cx + d = 0 \quad \rightarrow \quad t^3 + pt + q = 0$$

where

$$p = \frac{3ac - b^2}{3a^2}, \quad q = \frac{2b^3 - 9abc + 27a^2d}{27a^3}.$$

In our case,

$$p = -\frac{-36 - 25MB^2}{27B^2},$$
$$q = \frac{-250M^3B^2 + 2376M}{729B^2}.$$

Therefore

$$\Delta = -4(-\frac{36 + 25MB^2}{27B^2})^3 - 27(\frac{-250M^3B^2 + 2376M}{729B^2})^2. \tag{4.2}$$

We have 3 and 1 real roots of the Eq. (3.24) for $\Delta > 0$ and $\Delta < 0$, respectively. It can be shown that

$$\begin{cases} \Delta > 0, & \text{if } -375B^4M^4 + 1352B^2M^2 - 48 < 0 \\ \Delta < 0, & \text{if } -375B^4M^4 + 1352B^2M^2 - 48 > 0 \end{cases} \tag{4.3}$$

where the condition above can be derived from the square-root terms in our roots (3.29).

4.3 Range of B Governing the Number of Real Roots

The above inequality determines the range of B values for which all three roots are real. Solving

$$-375B^4M^4 + 1352B^2M^2 - 48 > 0, \tag{4.4}$$

for B gets us

$$\frac{\sqrt{\frac{1}{375}(676 - 152\sqrt{19})}}{M} < B < \frac{\sqrt{\frac{1}{375}(676 + 152\sqrt{19})}}{M}. \tag{4.5}$$

Approximating these values

$$\frac{0.189366386}{M} < B < \frac{1.889305085}{M}. \tag{4.6}$$

We call these limits, B_1 and B_2,

$$B_1 = \frac{0.189366386}{M}, \quad B_2 = \frac{1.889305085}{M}. \tag{4.7}$$

Therefore, we can summarize our results as follows:

$$\begin{cases} 3 \text{ real roots} & \text{if } B < B_1 \text{ or } B > B_2 \\ 1 \text{ real root} & \text{if } B_1 < B < B_2 \end{cases} \tag{4.8}$$

We will visualize these results through various plots of r as a function of B. However, first, we include a brief discussion of the effective potential.

4.4 Effective Potential

For lightlike geodesics in the equatorial plane, Dhurandhar and Sharma [Dhurandhar and Sharma (1983)] define an effective potential

$$V_{\text{eff}} = \frac{\Lambda^4}{r^2}\left(1 - \frac{2M}{r}\right), \tag{4.9}$$

that satisfies the orbital equation

$$\left(\frac{dr}{d\phi}\right)^2 = \frac{r^4}{\Lambda^8}\left(\frac{E^2}{L^2} - V_{\text{eff}}\right). \tag{4.10}$$

V_{eff} is plotted in Fig. (4.1) for various B values. It can be observed that V_{eff} starts

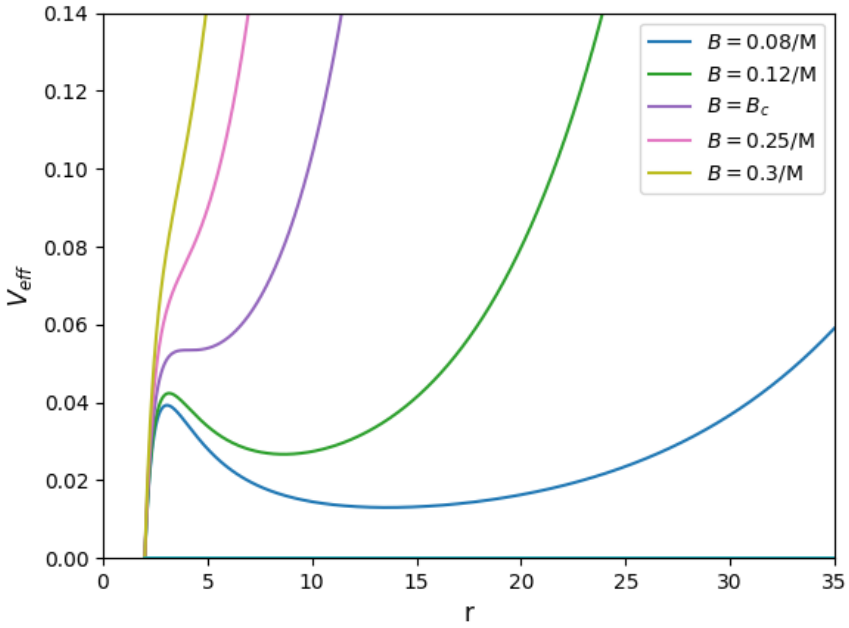

Figure 4.1: Equatorial effective potential V_{eff} from Eq. (4.9) vs. r for various B values. Here we give r in units of M and V_{eff} in units of $1/M^2$.

at $-\infty$ for $r = 2M$ and goes to ∞ for $r = \infty$. In between, for $B < B_1$, we have two extrema, corresponding to r_1 and r_2 that can be obtained by solving for

$$\frac{\partial V_{\text{eff}}}{\partial r} = 0 \tag{4.11}$$

As we will later see, r_2 corresponds to the unstable equilibrium point which occurs at a smaller r value than r_1 which is the stable equilibrium point.

For all values of $B < B_1$, we have two critical points: r_1 and r_2. If B increases from 0 to B_1, r_1 decreases from infinity to a limiting value r_c while r_1 increases from $3M$ to r_c, where

$$r_c \approx 4.119632981\, M \tag{4.12}$$

corresponds to a saddle point where $\partial^2 V_{\text{eff}}/\partial r^2$ is zero, indicating that it is neither a maximum nor a minimum. The plots for $B = 0.25/M, 0.3/M$ in Fig. 4.1 represent this case.

Now, we are ready for our discussion on the behavior of our circular lightlike geodesics with changing magnetic field strength B.

4.5 Graphical Analysis

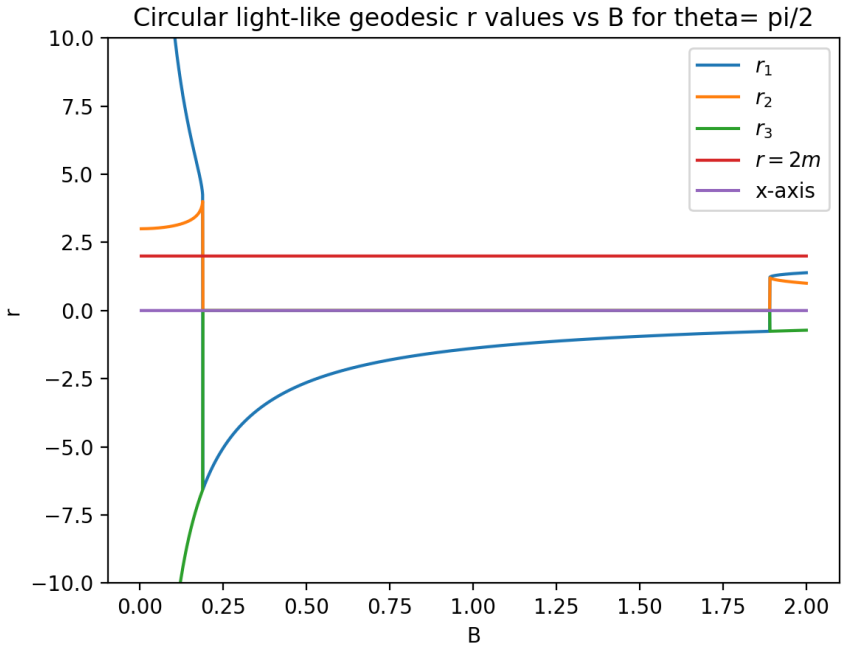

Figure 4.2: Circular lightlike geodesic r values vs. B. Here we give r in units of M and B in units of $1/M$.

Fig. 4.2 shows how the radii of circular orbits depend on B. We expect three real roots for B smaller than $0.18/M$ or larger than $1.8/M$, while only one real root for B in this critical range.

It can be seen that r_1 is the only solution to our cubic equation (3.24) that is real for all values of B. However, it is positive when the magnetic field strength B is outside the critical B range (4.6). Similarly, r_2 is real and positive outside the critical B range. r_3, however, is negative when real. Within the critical B range, r_2 and r_3 are complex and conjugates of each other.

In Fig. 4.2 we also plotted the event horizon at $r = 2M$ ($G = c = 1$). It can be observed that $B > B_2$, r_1 and r_2 are smaller than $2M$. However, note that in the domain $0 < r < 2M$, any hypersurface with r-constant is spacelike. So, a lightlike curve cannot be orthogonal to it. This means that the real solutions of the cubic equation for $B > B_2$ cannot represent circular lightlike geodesics. This is evident from the fact that when the value of L^2/E^2 from Eq. (3.17) is calculated for these solutions, it comes out as negative meaning that such a solution cannot exist. Therefore, we can define B_1 as

the critical value of the magnetic field strength (from now on referred to as B_c) beyond which no circular lightlike geodesics are possible.

In the Schwarzschild case, we have only one radial value for the circular lightlike geodesics at $r = 3M$ also called the *photon sphere*. This is the radius where we have circular lightlike geodesics passing through each point. Because of the spherical symmetry, these geodesics exist for all θ values. Since the Ernst spacetime reduces to the Schwarzschild spacetime for $B \to 0$, we would expect that, in this limit, our circular geodesic r_2 would converge to this value and r_1 to shift to infinity. This is obvious from Fig. 4.2. Here, $r_1 \to \infty$, $r_2 \to 3M$ while $r_3 \to -\infty$ the closer you get to the r-axis, i.e., $B \to 0$.

4.6 Stability of Circular Lightlike Geodesics with respect to coordinate r

A circular orbit is stable along the radial coordinate r if a small radial perturbation causes oscillatory motion around the equilibrium position. Conversely, if small perturbations lead to divergence from the orbit, it is unstable. Mathematically, this stability is determined by the second derivative of the effective potential:

$$\frac{\partial^2 V_{\text{eff}}}{\partial r^2} > 0 \quad \text{(Stable)},$$
$$\frac{\partial^2 V_{\text{eff}}}{\partial r^2} < 0 \quad \text{(Unstable)}$$

The second derivative of the effective potential is evaluated as follows:

$$\frac{\partial^2 V_{\text{eff}}}{\partial r^2} = \frac{(B^2r^2+4)^2\left[3r\left(5B^4r^4-8B^2r^2+16\right)-4M\left(5B^4r^4-16B^2r^2+48\right)\right]}{128r^5} \tag{4.13}$$

4.6.1 Stability of r_1

It can be shown numerically that r_1 is always stable with respect to the radial coordinate. Therefore, unlike the Schwarzschild spacetime, the Ernst spacetime with a non-zero magnetic field strength B admits stable circular light-like geodesics as well.

4.6.2 Stability of r_2

Our results confirm that the second circular orbit, r_2, is always unstable with respect to the radial coordinate. This finding is expected, as r_2 originates from the Schwarzschild photon sphere at $r = 3M$, which is known to be an unstable equilibrium. The Schwarzschild case corresponds to $B = 0$, and in the limit of small B, r_2 smoothly deforms from this photon sphere.
Since the photon sphere is always unstable in Schwarzschild spacetime, its counterpart in the Ernst spacetime remains unstable for all values of B.

4.7 Stability of Circular Lightlike Geodesics with respect to coordinate θ

Now we will examine the stability of the circular lightlike geodesics along the θ coordinate. The second derivative of the effective potential is evaluated as follows:

$$\frac{\partial^2 V_{\text{eff}}}{\partial\theta^2} = \frac{1}{32r}\Big[B^2(2M-r)\left(B^2r^2\sin^2\theta+4\right)^2\Big(\sin^2\theta\left(B^2r^2\sin^2\theta+4\right) - \cos^2\theta\left(7B^2r^2\sin^2\theta+4\right)\Big)\Big],$$

which evaluated for $\theta = \pi/2$ gets us

$$\left.\frac{\partial^2 V_{\text{eff}}}{\partial\theta^2}\right|_{\theta=\pi/2} = \frac{B^2(2M-r)\left(B^2r^2+4\right)^3}{32r}. \tag{4.14}$$

It can be shown that the above expression is positive for r_1 and r_2 indicating that our circular lightlike geodesics are always stable with respect to the θ coordinate.

4.8 Conclusion

In this chapter, we analyzed the numerical solutions and properties of circular lightlike geodesics about the z-axis in Ernst spacetime, focusing on their dependence on the magnetic field strength B. We found that the number of circular photon orbits in Ernst spacetime depends critically on the magnetic field strength B, corresponding to the critical points of V_{eff}. For $B < B_c$ we have two critical points. For $B > B_c$, r_1 and r_2 merge into a saddle point. We identified a critical magnetic field strength B_c beyond which no circular orbits exist. When the B is smaller than B_c we have two physical solutions to the cubic equation (3.24), r_1 and r_2. r_1 is stable when real and outside the event horizon, a feature absent in Schwarzschild spacetime. r_2 is always unstable, similar to the Schwarzschild photon sphere ($r = 3M$). All circular orbits are stable under perturbations in the θ direction.

Chapter 5

Angular Deflection

5.1 Introduction

In this chapter, we explore the exact angular deflection formula for null geodesics restricted in the meridional and equatorial planes of the Ernst spacetime and shadow formation. By exploiting the conformal relationship between the Ernst and Schwarzschild metrics in the meridional plane, we derive an effective angular deflection formula expression for null geodesics. With three conserved quantities, the $(2+1)$-dimensional spacetime is fully integrable. We then contrast this with light trajectories constrained to the equatorial plane, where the magnetic field explicitly influences the motion.

5.2 Conformal Relationship with Schwarzschild Spacetime

Recall from Sec. 3.5, the Ernst metric is conformal to the Schwarzschild metric reduced to the meridional plane with Λ^2 the conformal factor. This means that the trajectories of lightlike geodesics in the meridional planes of the two spacetimes are the same. We have a $(2+1)$-dimensional system in the meridional plane and 3 conserved quantities: $E, \tilde{L}$ and $\mathcal{L}$. This makes the geodesic equations fully integrable.

5.3 Angular Deflection in a Meridional Plane

Using Eqs. (3.37) and (3.38) in the Lagrangian (3.31) we have

$$-\frac{E^2}{\left(1-\frac{2M}{r}\right)}+\frac{1}{\left(1-\frac{2M}{r}\right)}\dot{r}^2+\frac{\tilde{L}^2}{r^2}=0,$$

$$\dot{r}^2=E^2-\left(1-\frac{2M}{r}\right)\frac{\tilde{L}^2}{r^2} \tag{5.1}$$

From Eq. (3.38)

$$\dot{\tilde{\phi}}^2=\frac{\tilde{L}^2}{r^4} \tag{5.2}$$

Dividing Eq. (5.1) by the above equation gets us

$$\left(\frac{dr}{d\tilde{\phi}}\right)^2 = \frac{E^2}{\tilde{L}^2}r^4 - r^2 + 2Mr. \tag{5.3}$$

If the light ray goes through a minimum r value at r_m, we have

$$\left(\frac{dr}{d\tilde{\phi}}\right)\Bigg|^2_{r=r_m} = \frac{E^2}{\tilde{L}^2}r_m^4 - r_m^2 + 2Mr_m = 0,$$

$$\frac{E^2}{\tilde{L}^2} = \frac{1}{r_m^2} - \frac{2M}{r_m^3}. \tag{5.4}$$

Using this expression in Eq. (5.3)

$$\frac{d\tilde{\phi}}{dr} = \frac{1}{\sqrt{\left(\frac{1}{r_m^2} - \frac{2M}{r_m^3}\right)r^4 - r^2 + 2Mr}},$$

$$\frac{d\tilde{\phi}}{dr} = \frac{r_m}{\sqrt{\left(1 - \frac{2M}{r_m}\right)r^4 - r^2r_m^2 + 2Mrr_m^2}}.$$

Integrating over a light ray yields the angular deflection relation in the meridional plane

$$\delta_{\text{mrd}} = 2\int_{r_m}^{\infty} \frac{r_m}{\sqrt{\left(1 - \frac{2M}{r_m}\right)r^4 - r^2r_m^2 + 2Mrr_m^2}}dr. \tag{5.5}$$

This expression is plotted in Fig. 5.1. The expression goes to infinity for $r = 3M$, as expected from a comparison with the Schwarzschild case.

5.4 Angular Deflection in the Equatorial Plane

Now, we evaluate the angular deflection for a constant θ, for a light ray restricted to the equatorial plane

$$\sin\theta = 1, \quad \dot{\theta} = 0.$$

The Lagrangian is given by

$$\mathcal{L} = \frac{1}{2}\left[- \Lambda^2_{\theta=\pi/2}(1 - \frac{2M}{r})\dot{t}^2 + \frac{\Lambda^2_{\theta=\pi/2}}{(1 - \frac{2M}{r})}\dot{r}^2 + \frac{r^2}{\Lambda^2_{\theta=\pi/2}}\dot{\phi}^2\right]. \tag{5.6}$$

The conserved quantities are

$$\frac{\partial\mathcal{L}}{\partial\dot{t}} = p_t = -E = \Lambda^2_{\theta=\pi/2}\left(1 - \frac{2M}{r}\right)\dot{t}, \tag{5.7}$$

$$\frac{\partial\mathcal{L}}{\partial\dot{\phi}} = p_\phi = L = \frac{r^2}{\Lambda^2_{\theta=\pi/2}}\dot{\phi}, \tag{5.8}$$

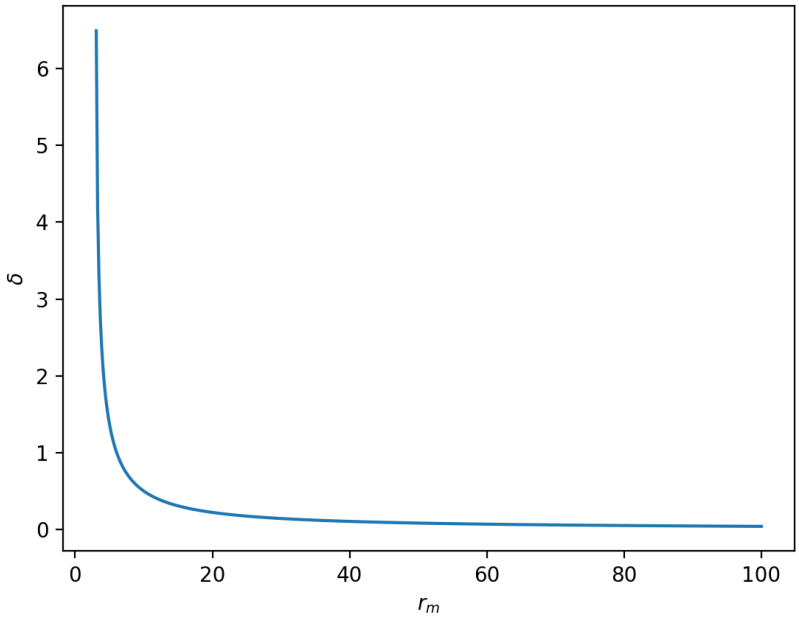

Figure 5.1: Angular deflection δ_{mrd} in the meridional plane against the minimum r value r_m. Here we give r_m in units of M and δ in radians.

Using these definitions in the expression for the Lagrangian

$$-\frac{E^2}{\Lambda^2_{\theta=\pi/2}\left(1-\frac{2M}{r}\right)}+\frac{\Lambda^2_{\theta=\pi/2}}{r^2}L^2+\frac{\Lambda^2_{\theta=\pi/2}}{\left(1-\frac{2M}{r}\right)}L^2=0,$$

$$\dot{r}^2=\frac{1}{\Lambda^4_{\theta=\pi/2}}E^2-\frac{\left(1-\frac{2M}{r}\right)}{r^2}L^2.$$

From the definition of L in Eq. (5.8) we have

$$\dot{\phi}^2=\frac{L^2\Lambda^4_{\theta=\pi/2}}{r^4}. \tag{5.9}$$

Dividing the two expressions and solving

$$\frac{\dot{r}^2}{\dot{\phi}^2}=\left(\frac{dr}{d\phi}\right)^2=\frac{r^4}{L^2\Lambda^4_{\theta=\pi/2}}\left(\frac{1}{\Lambda^4_{\theta=\pi/2}}E^2-\frac{\left(1-\frac{2M}{r}\right)}{r^2}L^2\right),$$

$$\left(\frac{dr}{d\phi}\right)^2=\frac{r^4}{\Lambda^8_{\theta=\pi/2}}\frac{E^2}{L^2}-\frac{r^2\left(1-\frac{2M}{r}\right)}{\Lambda^4_{\theta=\pi/2}}.$$

$$\frac{d\phi}{dr}=\left[\frac{r^4}{\Lambda^8}\left(\frac{E^2}{L^2}-\frac{\Lambda^4\left(1-\frac{2M}{r}\right)}{r^2}\right)\right]^{-1/2}. \tag{5.10}$$

If the ray light has a close approach at r_m

$$\left(\frac{dr}{d\phi}\right)\Big|^2_{r=r_m}=\frac{r_m^4}{\Lambda_m^8}\frac{E^2}{L^2}-\frac{r_m^2\left(1-\frac{2M}{r_m}\right)}{\Lambda_m^4}=0.$$

Thus we have

$$\frac{E^2}{L^2} = \frac{\Lambda_m^4 \left(1 - \frac{2M}{r_m}\right)}{r_m^2}, \tag{5.11}$$

Eq. (5.10) thus becomes

$$d\phi = dr \left[\frac{r^4}{\Lambda^8} \left(\frac{\Lambda_m^4 \left(1 - \frac{2M}{r_m}\right)}{\Lambda^4 r_m^2} - \frac{\Lambda^4 \left(1 - \frac{2M}{r}\right)}{r^2} \right) \right]^{-1/2}.$$

Integrating over a light ray yields the angular deflection formula

$$\delta_{\text{eqt}} = 2 \int_{r_m}^{\infty} \frac{r_m}{\sqrt{\frac{\Lambda_m^4}{\Lambda^8} \left(1 - \frac{2M}{r_m}\right) r^4 - \frac{r^2 r_m^2}{\Lambda^4} + \frac{2M r r_m^2}{\Lambda^4}}} dr. \tag{5.12}$$

However, once we evaluate the expression inside the square root, for any $r < r_m$, it comes out as negative. This means that the notion of angular deflection in the equatorial plane has no physical relevance. In other words, a light ray that goes through a minimum radial distance r_m around a Schwarzschild-Melvin black hole cannot escape to infinity. We had provided this result in Sec. 2.4 and it is an extension of the result provided by Dhurandhar et al. that states that for $B > 0$, no geodesics with non-zero angular momentum ($L \neq 0$) can reach infinity [Dhurandhar and Sharma (1983)]. Since geodesics can go through a minimum radial distance r_m only if the angular momentum is non-zero, such a light ray cannot escape to infinity, and hence our interpretation of angular deflection in the equatorial plane is not relevant.

5.5 Conclusion

We have derived expressions for the angular deflection of light rays in both the meridional and equatorial planes of the Ernst spacetime. The conformal equivalence with Schwarzschild spacetime in the meridional plane simplifies the analysis and reveals that light bending resembles that in Schwarzschild black holes. However, in the equatorial plane, the magnetic field modifies the effective potential and trajectory of light, making the angular deflection and shadow shape dependent on the field strength. There exist bound orbits at $r = 3M$ for each meridional plane and light rays with a non-zero angular momentum L cannot escape to infinity.

Chapter 6

Shadow Diameter

6.1 Introduction

The "shadow" of a black hole is the dark silhouette cast against a backdrop of glowing matter or radiation. Photons near the photon sphere or the photon orbits at $r = 3M$ can be captured or deflected so strongly that they never reach the observer, producing a sharp-edged dark region in the image. Observationally, the shadow's size and shape encode key properties of the spacetime in the strong-gravity regime.

In a general axisymmetric spacetime like the Ernst solution, only three constants of motion exist for null geodesics: energy E, the z-component of the angular momentum L and the Lagrangian $\mathcal{L} = 0$. Absent a fourth Carter-like constant, the spacetime is chaotic, and hence, the shadow boundary cannot be obtained analytically for arbitrary inclinations. However, by restricting to the meridional ($\dot{\phi} = 0$) and equatorial ($\theta = \pi/2$) planes, the system effectively reduces to $(2 + 1)$ dimensions with three conserved quantities. In each of those planes, one can then solve explicitly for the vertical and horizontal angular radii of the shadow as seen by an observer far away.

Here we define two characteristic shadow angles: α for light confined to the meridional plane ($\dot{\phi} = 0$) and β for light confined to the equatorial plane ($\dot{\theta} = 0$).

6.2 Vertical Angular Radius

It is necessary to specify where the light sources are and we must consider all of the initial radii of the sources r_S with all possible initial directions of past-oriented light rays from the observer position. As earlier discussed in Sec. 2.4, the Ernst spacetime is not asymptotically flat, hence any photon with $L \neq 0$ falls back inwards [Dhurandhar and Sharma (1983)]. Therefore, we assume light sources at a large but finite radius r_S (instead of at infinity). The observer (at radius r_O) will then see bright regions in the sky corresponding to directions where backward-traced rays hit these sources, and dark (shadow) regions where rays either fall into the black hole or remain trapped.

For light rays in the meridional plane, $\dot{\phi} = 0$ and we have

$$\tan\alpha = \frac{r}{\left(1-\frac{2M}{r}\right)^{-1/2}} \frac{d\tilde{\theta}}{d\tilde{r}}\bigg|_{r=r_O},$$
$$\tan^2\alpha = \frac{r^2}{\left(1-\frac{2M}{r}\right)^{-1}} \left(\frac{d\tilde{\theta}}{d\tilde{r}}\right)^2\bigg|_{r=r_O},$$

where r_O is the observer's radius that is assumed to be static. Using Eq. (5.3)

$$\tan^2\alpha = \frac{r_O^2\left(1-\frac{2M}{r_O}\right)}{\frac{E^2}{\tilde{L}^2}r_O^4 - r_O^2 + 2Mr_O},$$
$$\tan^2\alpha = \frac{(r_O-2M)}{\frac{E^2}{\tilde{L}^2}r_O^3 - (r_O-2M)},$$
$$\frac{1}{\tan^2\alpha} = \frac{E^2 r_O^3}{\tilde{L}^2(r_O-2M)} - 1.$$

From simple trigonometry, we get

$$\sin^2\alpha = \frac{\tilde{L}^2(r_O-2M)}{E^2 r_O^3}. \tag{6.1}$$

Much like the Schwarzschild case, where we can obtain the ratio of the constants of motion L/E for the photon sphere, we can obtain the value of $\tilde{L}/E$ by evaluating the presence of circular geodesics in the meridional plane of the Ernst solution. The ratio $\tilde{L}/E$ for this light ray is the same as that for the circular light ray.

We showed in Sec. 3.5.1 that there exist photon orbits in each meridional plane of the Ernst spacetime [Lima Junior et al. (2022)]. These orbits at $t = cte.$ span the 2-surface of the Schwarzschild-Melvin black hole geometry

$$ds^2\Big|_{t=cte.,r=3M} = (3M)^2\left[\Lambda^2 d\theta^2 + \frac{\sin^2\theta}{\Lambda^2}d\phi^2\right]. \tag{6.2}$$

Inserting $r = 3M$ in Eq. (3.39) get us

$$\frac{\tilde{L}^2}{E^2} = 27M^2. \tag{6.3}$$

Using this expression in Eq. (6.1)

$$\sin^2\alpha = \frac{27M^2(r_O-2M)}{r_O^3}. \tag{6.4}$$

This expression provides the vertical angular radius of the Schwarzschild-Melvin black hole. Note that this coincides with the expression obtained for the angular radius of the Schwarzschild black hole shadow. Here, the conserved quantity $\tilde{L}$ plays the role of angular momentum L in the Schwarzschild case. Note that this expression is independent of the observer's ϑ-coordinate and is hence valid for all observers with $3M < r_O < r_S$.

6.3 Horizontal Angular Radius

Now, for the horizontal angular radius of the shadow, we restrict to the equatorial plane ($\theta = \pi/2$). Hence, the Lagrangian is given by

$$\mathcal{L} = \frac{1}{2}\Bigg[- \Lambda^2_{\theta=\pi/2}(1 - \frac{2M}{r})\dot{t}^2 + \frac{\Lambda^2_{\theta=\pi/2}}{(1 - \frac{2M}{r})}\dot{r}^2 + \frac{r^2}{\Lambda^2_{\theta=\pi/2}}\dot{\phi}^2\Bigg]. \tag{6.5}$$

Thus, we have

$$\tan\beta = \frac{r}{\Lambda^2_O\left(1-\frac{2M}{r}\right)^{-1/2}}\frac{d\phi}{dr}\bigg|_{r=r_O},$$
$$\tan^2\beta = \frac{r^2\left(1-\frac{2M}{r}\right)}{\Lambda^4_O}\left(\frac{d\phi}{dr}\right)^2\bigg|_{r=r_O}.$$

Using Eq. (5.10)

$$\tan^2\beta = \frac{\frac{r_O^2\left(1-\frac{2M}{r_O}\right)}{\Lambda^4_O}}{\frac{r_O^4}{\Lambda^8_O}\left(\frac{E^2}{L^2} - \frac{\Lambda^4_O\left(1-\frac{2M}{r_O}\right)}{r_O^2}\right)},$$
$$\tan^2\beta = \frac{\left(1-\frac{2M}{r_O}\right)}{\frac{r_O^2}{\Lambda^4_O}\left(\frac{E^2}{L^2} - \frac{\Lambda^4_O\left(1-\frac{2M}{r_O}\right)}{r_O^2}\right)}.$$

Inverting the expression gets us

$$\frac{\cos^2\beta}{\sin^2\beta} = \frac{\frac{r_O^2}{\Lambda^4_O}\left(\frac{E^2}{L^2} - \frac{\Lambda^4_O\left(1-\frac{2M}{r_O}\right)}{r_O^2}\right)}{\left(1-\frac{2M}{r_O}\right)},$$
$$\frac{\cos^2\beta}{\sin^2\beta} + 1 = \frac{\frac{r_O^2}{\Lambda^4_O}\left(\frac{E^2}{L^2} - \frac{\Lambda^4_O\left(1-\frac{2M}{r_O}\right)}{r_O^2}\right)}{\left(1-\frac{2M}{r_O}\right)} + 1,$$
$$\frac{1}{\sin^2\beta} = \frac{\frac{r_O^2}{\Lambda^4_O}\left(\frac{E^2}{L^2} - \frac{\Lambda^4_O\left(1-\frac{2M}{r_O}\right)}{r_O^2}\right) + \left(1-\frac{2M}{r_O}\right)}{\left(1-\frac{2M}{r_O}\right)},$$
$$\sin^2\beta = \frac{\left(1-\frac{2M}{r_O}\right)}{\frac{r_O^2}{\Lambda^4_O}\left(\frac{E^2}{L^2} - \frac{\Lambda^4_O\left(1-\frac{2M}{r_O}\right)}{r_O^2}\right) + \left(1-\frac{2M}{r_O}\right)},$$
$$\sin^2\beta = \frac{(r_O - 2M)}{\frac{r_O^3}{\Lambda^4_O}\left(\frac{E^2}{L^2} - \frac{\Lambda^4_O(r_O-2M)}{r_O^3}\right) + (r_O - 2M)}.$$

Finally, we have

$$\sin^2\beta = \Lambda_O^4 \frac{\frac{L^2}{E^2}(r_O - 2M)}{r_O^3},$$

where the value of L^2/E^2 depends on the positioning of the observer and the light sources.

We plot the effective potential given by Eq. (4.9) for $B = 0.12/M$ in Fig. (6.2). We read that there is a critical observer radius coordinate r'_O with $r_2 < r_1 < r'_O$, determined by

$$V_{\text{eff}}(r_2) = V_{\text{eff}}(r'_O)\,, \tag{6.6}$$

where V_{eff} is given by Eq. (4.9). The radius value r'_O is marked by a red dotted line in Figs. 6.1 and 6.2.

6.3.1 Case 1: $r_S < r'_O$

First, we consider the case where the light sources are placed inside r'_O, i.e. $r_2 < r_O < r_S < r'_O$. In this case, trajectories with $E^2/L^2 \geq V_{\text{eff}}|_{r_2}$ will be reflected outwards (bright region) and those with $E^2/L^2 \approx V_{\text{eff}}|_{r_1}$ will be trapped in bound oscillatory orbit (dark regions). Those with $E^2/L^2 = V_{\text{eff}}|_{r_2}$ will spiral around r_2 and then go to the horizon and provide the horizontal shadow boundary.

Using the value of L^2/E^2 for the circular lightlike geodesics in the equatorial plane from Eq. (3.17), we obtain

$$\sin^2\beta = \frac{\Lambda^4(r_O, \pi/2)(r_O - 2M)r_2^3}{\Lambda^4(r_2, \pi/2)(r_2 - 2M)r_O^3}. \tag{6.7}$$

This expression provides the horizontal angular radius of the Schwarzschild-Melvin black hole for the case $r_S < r'_O$. Note that for $B \to 0$, $\Lambda \to 1$ and the above expression reduces to the angular radius of the Schwarzschild black hole. β has a maximum of $\pi/2$ when the observer radius $r_O = r_2$. As r_O moves outwards, β decreases to a minimum before rising to the maximum value of $\pi/2$ again at r'_O.

We consider another possibility when the light sources lie in the domain $r_1 < r_S < r'_O$ such that the potential at r_S satisfies $V_{\text{eff}}(r_1) < V_{\text{eff}}(r_S) < V_{\text{eff}}(r_2)$. In this case, there is a second radius $r'_S \in (r_2, r_1)$ with

$$V_{\text{eff}}(r'_S) = V_{\text{eff}}(r_S)\,.$$

This case is depicted in Fig. 6.1 where r_S and r'_S are marked by the blue and green vertical lines, respectively. Consequently, an observer located at any radius $r_O \in (r'_S, r_S)$ finds that past-directed rays with

$$\frac{E^2}{L^2} < V_{\text{eff}}(r_S)$$

cannot reach the light sources at r_S; these rays remain trapped or fall inward and thus produce a dark patch on the observer's sky. The boundary of that patch is given by the rays with the critical value $E^2/L^2 = V_{\text{eff}}(r_S)$. Note that the inner matching radius r'_S exists only when $V_{\text{eff}}(r_S)$ lies strictly between the local minimum and local maximum of V_{eff}; if $V_{\text{eff}}(r_S) \leq V_{\text{eff}}(r_1)$ or $V_{\text{eff}}(r_S) \geq V_{\text{eff}}(r_2)$ no such inner solution in (r_2, r_1) exists.

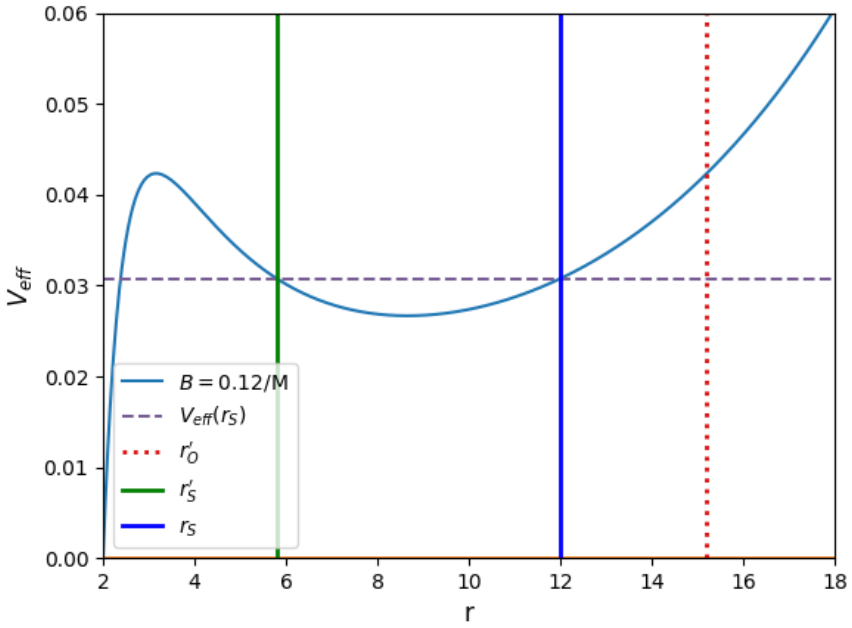

Figure 6.1: Equatorial effective potential V_{eff} for $B = 0.12/M$ for $r_1 < r_s < r'_O$. Here we give r in units of M and V_{eff} in units of $1/M^2$.

6.3.2 Case 2: $r'_O < r_S$

Now we consider the case of the light sources placed outside the critical observer radius r'_O. For $r_S > r'_O$ (represented by the blue vertical line in Fig. 6.2), we define a critical value of the effective potential

$$V_{\text{eff}}(r_S) = \left.\frac{E^2}{L^2}\right|_{\text{crit}}$$

corresponding to the point where the vertical line $r = r_S$ meets the plot of the potential. Hence, the light rays with $E^2/L^2 < E^2/L^2\big|_{\text{crit}}$ never reach r_S, so we associate darkness with these light rays, , i.e., Eq. (6.7) wouldn't be true so, in this case β is bigger than $\pi/2$ giving us the following equation for the horizontal component of the shadow

$$\sin^2\beta = \frac{\Lambda^4(r_O, \pi/2)(r_O - 2M)r_S^3}{\Lambda^4(r_S, \pi/2)(r_S - 2M)r_O^3}. \tag{6.8}$$

The shape of this equation is similar to Eq. (6.7) except that the constants, L/E are now evaluated at r_S instead of r_2.

The two angular radii are plotted as a function of the observer radius r_O for $B = 0.1/M$ ($r'_O = 21.12M$) for the two cases of $r'_O > r_S$ and $r'_O < r_S$ in Fig. (6.3).

6.4 Geometry of the Shadow

In this section, we show analytically that the shadow of a Schwarzschild-Melvin black hole is oblate, i.e., $\beta > \alpha$. We compare the expressions for the horizontal and vertical

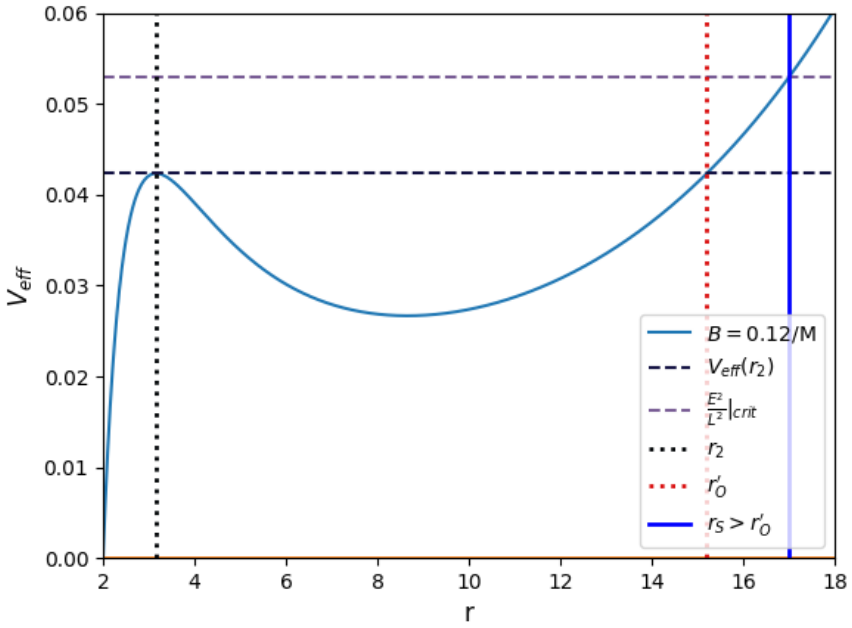

Figure 6.2: Equatorial effective potential V_{eff} from Eq. (4.9) vs. r for $B = 0.12/M$. Here we give r in units of M and V_{eff} in units of $1/M^2$.

angular radii. For the case $r_2 < r_O < r_S < r'_O$, $\alpha, \beta \in [0, \pi/2]$ (Fig. 6.3). Thus, we need to show $\sin^2\beta > \sin^2\alpha$ which translates to proving that

$$\frac{\Lambda_O^4 r_2^3}{\Lambda_{r_2,\,\theta=\pi/2}^4 (r_2 - 2M)} > 27M^2.$$

For an observer located at $r_O > r_2$ for $B \neq 0$

$$\frac{\Lambda_O^4}{\Lambda_{r_2,\,\theta=\pi/2}^4} > 1. \tag{6.9}$$

We have seen that $r_2 > r = 3M$ so if we represent r_2 as

$$r_2 = (3 + \epsilon)M,$$

where $\epsilon \ll 1$. Hence

$$\frac{r_2^3}{r_2 - 2M} = \frac{(3+\epsilon)^3 M^3}{(1+\epsilon)M},$$
$$\frac{r_2^3}{r_2 - 2M} = \frac{27M^2(1 + \frac{\epsilon}{3})^3}{(1+\epsilon)}.$$

Using binomial series expansion in the numerator and ignoring the higher-order terms

$$\frac{r_2^3}{r_2 - 2M} = 27M^2. \tag{6.10}$$

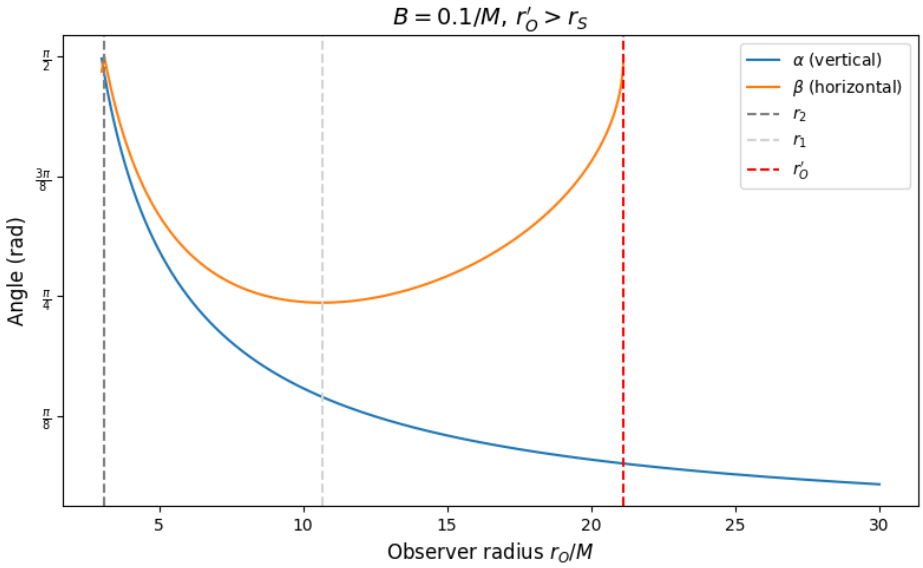

(a) r_S anywhere $r_2 < r_S < r'_O$.

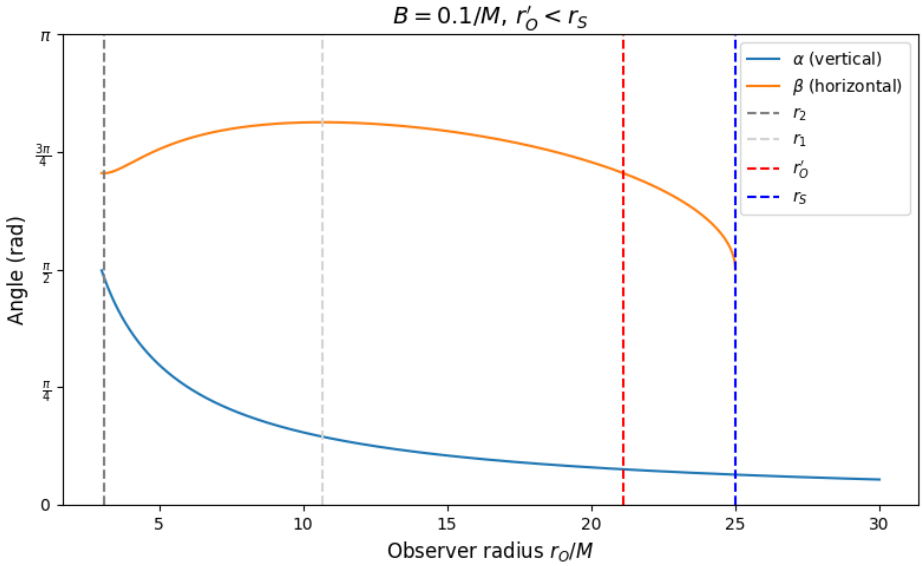

(b) $r_S = 25M$ above r'_O.

Figure 6.3: Shadow vertical and horizontal angular radii vs. observer distance r_O in the equatorial plane.

From Eq. (6.9)

$$\frac{\Lambda_O^4 r_2^3}{\Lambda_{r_2,\,\theta=\pi/2}^4 (r_2 - 2M)} > 27M^2. \tag{6.11}$$

This implies that the horizontal angular radius of the Schwarzschild–Melvin black hole exceeds its vertical angular radius ($\beta > \alpha$), confirming that the shadow exhibits an oblate shape.

Next, for the case of $r'_O < r_S$, Fig. 6.3 shows that for all observer positions between r_2 and r_S, the horizontal radius β is bigger than $\pi/2$ while the vertical radius α is smaller than $\pi/2$, so the statement that $\beta > \alpha$ is true in this case as well. This analytical result is consistent with the numerical findings of Junior et al. [Lima Junior et al. (2022)].

6.5 Conclusion

In this chapter, we derive analytic expressions for the angular radii of the Schwarzschild-Melvin black hole shadow by exploiting the meridional and equatorial reductions, where sufficient constants of motion are available. Due to conformal equivalence, the vertical angular radius matches that of the Schwarzschild black hole's angular radius. The conserved quantity $\tilde{L}$ obtained from the cyclicity of the θ coordinate plays the role of the angular momentum L from the Schwarzschild spacetime. The expression for horizontal angular radius reduces to that for a Schwarzschild black hole for $B \to 0$.

Chapter 7

Photon Rings

7.1 Introduction

Photon rings are thin, bright, infinite sequences of images of sources around the black holes due to light rays that orbit the black hole multiple times before reaching a distant observer [Gralla et al. (2019)]. They are composed of photons on near-bound orbits, and their formation is intimately tied to the presence of bound lightlike geodesics which correspond to a photon sphere in spherically symmetric spacetimes like the Schwarzschild [Claudel et al. (2001)]. However, in more general, axisymmetric or magnetized spacetimes, the geometry can be complex, and the existence of such bound trajectories requires detailed investigation [Ernst (1976); Lima Junior et al. (2022)]. Photon rings are of significant observational interest, particularly in the context of black hole imaging efforts like the Event Horizon Telescope, because they encode information about the strong-field region close to the black hole.

In this chapter, we investigate the presence and properties of photon rings around the Schwarzschild-Melvin black hole. We assume the emitters of light rays in an accretion disk in the equatorial plane. While the problem of photon rings cannot be solved analytically for an observer at an arbitrary inclination, if we assume the observer to be at the pole, we can use the strong deflection formalism introduced by Bozza and Scrapetta [Bozza and Scarpetta (2007)] to study the properties of the photon rings.

We showed in Sec. 3.5 that there exist bounded photon orbits at $r = 3M$ in all the meridional planes of a Schwarzschild-Melvin black hole. We study the relevant effective potential and conserved quantities to determine the existence and location of candidate photon rings. Our goal is to assess how the external magnetic field affects the structure of these orbits. Finally, we analyze the gap parameter, which is the relative distance between two consecutive photon rings.

7.2 Photon Rings Formalism

Working in a spherically symmetric spacetime,

$$ds^2 = -A(r)c^2dt^2 + B(r)dr^2 + D(r)(d\theta^2 + \sin^2\theta d\phi^2) \tag{7.1}$$

Bozza and Scrapetta [Bozza and Scarpetta (2007)] showed that for an observer outside the photon sphere, the total range of the coordinate $\tilde{\phi}$ swept out by a light ray that,

starting at a light source at r_s, going through a minimum radius value R, and then arriving at an observer at r_O is given by

$$\Delta\tilde{\phi} = \int_R^{r_s} b\sqrt{\frac{B(r)}{D(r)\mathcal{R}(r,b)}} + \int_R^{r_O} b\sqrt{\frac{B(r)}{D(r)\mathcal{R}(r,b)}}, \tag{7.2}$$

where

$$\mathcal{R}(r,b) = \frac{D(r)}{A(r)} - b^2, \quad b = \left|\frac{p_{\tilde{\phi}}}{p_t}\right|. \tag{7.3}$$

For finite values of r_s and r_O, Bozza and Scrapetta [Bozza and Scarpetta (2007)] showed that the total angle swept out by the light ray is given by

$$\Delta\tilde{\phi} = -\tilde{a}\log\left(\frac{\epsilon}{\eta_O\eta_S}\right) + \tilde{a}\log\left(\frac{2\beta_{ph}}{b_{cr}^2}\right) + k_O + k_s, \tag{7.4}$$

where b_{cr} corresponds to the critical value of the constant $b = L/E$ evaluated at the photon sphere, i.e., the radius value where the light ray stays on the sphere with this radius if it starts tangentially to it.

$\tilde{a}$, η, k and β are given by

$$\tilde{a} = r_{ph}\sqrt{\frac{B(r_{ph})}{A(r_{ph})\beta_{ph}}}, \tag{7.5}$$

$$\eta_i = 1 - \frac{r_{ph}}{r_i}, \tag{7.6}$$

$$\beta = \frac{1}{2}r^2\frac{\partial^2\mathcal{R}(r,b)}{\partial r^2}, \tag{7.7}$$

$$k_i = \int_0^{\eta_i} g(\eta)d\eta, \tag{7.8}$$

where

$$g(\eta) = b_{cr}\sqrt{\frac{B(\eta)}{D(\eta)}}\frac{1}{\sqrt{\mathcal{R}(\eta,b_{cr})}}\frac{r_{ph}}{(1-\eta)^2} - \frac{b_{cr}}{\sqrt{\beta_{ph}}}\sqrt{\frac{B(r_{ph})}{D(r_{ph})}}\frac{r_{ph}}{|\eta|}. \tag{7.9}$$

Aratore, Tsupko and Perlick [Aratore et al. (2024)] provide an expression for the impact parameter expressed in terms of the azimuthal shift

$$b(\phi) = b_{cr}\left[1 + F(r_s)F(r_O)\exp\left(-\frac{\Delta\tilde{\phi}}{\tilde{a}}\right)\right], \tag{7.10}$$

where

$$F(r_i) = \sqrt{\frac{2\beta_{ph}}{b_{cr}^2}}\left(1 - \frac{r_{ph}}{r_i}\right)\exp\left(\frac{k_i}{\tilde{a}}\right), \tag{7.11}$$

$$\Delta\tilde{\phi} = (n+1)\pi - \cos^{-1}\left(\frac{\sin\phi}{\sqrt{\sin^2\phi + \cot^2\theta_O}}\right). \tag{7.12}$$

Here n corresponds to the number of half-turns the light ray makes around the black hole before reaching the observer. It could also be interpreted as the number of times

the light ray intersects the equatorial plane on the way to the observer. Primary image refers to order $n = 0$ when the light ray reaches the observer directly without any turn around the black hole. The image of order $n = 1$ refers to the case where the light ray makes a half-turn around the black hole. All the other images ($n \geq 2$) are called higher-order images. See Fig. 1 in Tsupko [Tsupko (2022)] for a better illustration.

Note that the above derivation is valid in the case of a spherically symmetric spacetime that has a photon sphere r_{ph}. However, since the Ernst spacetime reduced to a meridional plane is conformal to the Schwarzschild spacetime in the meridional plane, under appropriate conditions, we can use the above formalism to understand photon rings produced by a Schwarzschild-Melvin black hole.

Since there exist bound photon orbits in the Ernst spacetime in the meridional plane at $r = 3M$ we can use the formalism by Aratore, Tsupko and Perlick [Aratore et al. (2024)].

Inserting $F(r_i)$ from Eq. (7.11) into Eq. (7.10) gets us

$$b(\phi) = b_{cr}\left[1 + \frac{2\beta_{ph}}{b_{cr}^2}\left(1 - \frac{r_{ph}}{r_s}\right)\left(1 - \frac{r_{ph}}{r_O}\right)\exp\left(\frac{k_s + k_O}{\tilde{a}}\right)\exp\left(-\frac{\Delta\tilde{\phi}}{\tilde{a}}\right)\right], \tag{7.13}$$

where for a polar observer ($\theta_O = 0$), $\Delta\tilde{\phi}$ becomes

$$\Delta\tilde{\phi} = \left(n + \frac{1}{2}\right)\pi. \tag{7.14}$$

It can be shown that for the Schwarzschild or a conformal spacetime $\tilde{a} = 1$. Hence, we have

$$b_n = b_{cr}\left[1 + \frac{2\beta_{ph}}{b_{cr}^2}\left(1 - \frac{r_{ph}}{r_s}\right)\left(1 - \frac{r_{ph}}{r_O}\right)\exp\left(k_s + k_O\right)e^{-\left(n+\frac{1}{2}\right)\pi}\right]. \tag{7.15}$$

Note that we have not used the asymptotically flat condition for the spacetime. Aratore, Tsupko and Perlick apply this condition to obtain the expression for b_n for the case of an observer at infinity ($r_O \to \infty$). However, while keeping the observer at a finite distance, we can evaluate an expression for b_n.

7.3 Derivation of b_n

For a spacetime conformal to Schwarzschild, working with lightlike geodesics, with a suitable affine parameter transformation, we can use the same metric coefficients as in Schwarzschild

$$A(r) = B^{-1}(r) = 1 - \frac{2M}{r}, \quad D(r) = r^2.$$

The other quantities of interest are

$$r_{ph} = 3M,$$
$$b_{cr} = 3\sqrt{3}M,$$
$$\beta_{ph} = 81M^2,$$
$$\mathcal{R}(r, b) = \frac{r^2}{1 - \frac{2M}{r}} - b^2,$$
$$r = \frac{r_{ph}}{1 - \eta}.$$

Evaluating k from Eq. (7.8)

$$k_i = \int_0^{\eta_i} \left[b_{cr} \frac{1}{\sqrt{r(\eta)^2 \left(1 - \frac{2M}{r(\eta)}\right)}} \frac{1}{\sqrt{\frac{r(\eta)^2}{\left(1-\frac{2M}{r(\eta)}\right)} - b_{cr}^2}} \frac{r_{ph}}{(1-\eta)^2} - \frac{b_{cr}}{\sqrt{\beta_{ph}}} \frac{1}{\sqrt{1-\frac{2M}{r_{ph}}}} \frac{1}{\eta} \right] d\eta.$$

Inserting the values from above

$$k_i = \int_0^{\eta_i} \left[\frac{3\sqrt{3}M}{\frac{3M}{(1-\eta)}} \frac{1}{\sqrt{1-\frac{2M}{3M}(1-\eta)}} \frac{1}{\sqrt{\frac{\frac{9M^2}{(1-\eta)^2}}{1-\frac{2M}{3M}(1-\eta)} - 27M^2}} \frac{3M}{(1-\eta)^2} - \frac{3\sqrt{3}M}{9M} \frac{1}{\sqrt{1-\frac{2M}{3M}}} \frac{1}{\eta} \right] d\eta,$$

and resolving

$$k_i = \int_0^{\eta_i} \left[\frac{\sqrt{3}}{\sqrt{1-3(1-\eta)^2+2(1-\eta)^3}} - \frac{1}{\eta} \right] d\eta,$$

$$k_i = \sqrt{3} \int_0^{\eta_i} \frac{1}{\eta\sqrt{3-2\eta}} d\eta - \log \eta_i + \log 0.$$

Solving using an integral calculator gets us

$$k_i = \left[\log\left(\sqrt{3} - \sqrt{3-2\eta}\right) - \log\left(\sqrt{3} + \sqrt{3-2\eta}\right) \right] \Big|_o^{\eta_i} - \log \eta_i + \log 0 + \log C,$$

$$k_i = \log \left(\frac{2\sqrt{3}(\sqrt{3} - \sqrt{3-2\eta_i})}{\eta_i(\sqrt{3} + \sqrt{3-2\eta_i})} C \right),$$

$$k_i = \log \left(\frac{2\sqrt{3}C}{3 - \eta_i + \sqrt{9-6\eta_i}} \right).$$

We choose the additive constant C such that for $\eta_i \to 0$ we have $k_i \to 0$. $C = \sqrt{3}$ satisfies this need, getting us the following expression for k_i:

$$k_i = \log \left(\frac{6}{3 - \eta_i + \sqrt{9-6\eta_i}} \right). \tag{7.16}$$

Note that his expression reduces to that derived in Eq. (35) by Aratore, Tsupko and Perlick for an observer at infinity ($r_O \to \infty, \eta \to 1$).

$$k_O = \log \left(\frac{6}{2 + \sqrt{3}} \right). \tag{7.17}$$

Thus, inserting these values into the expression for b_n gets us, for a polar observer

$$b_n = 3\sqrt{3}M\left[1 + 6\left(1 - \frac{3M}{r_s}\right)\left(1 - \frac{3M}{r_O}\right)e^{-\left(n+\frac{1}{2}\right)\pi}\right.$$
$$\left.\left(\frac{6}{3 - \eta_s + \sqrt{9 - 6\eta_s}}\right)\left(\frac{6}{3 - \eta_O + \sqrt{9 - 6\eta_O}}\right)\right],$$

$$b_n = 3\sqrt{3}M\left[1 + 216\left(1 - \frac{3M}{r_s}\right)\left(1 - \frac{3M}{r_O}\right)\right.$$
$$\left.\frac{e^{-\left(n+\frac{1}{2}\right)\pi}}{\left(3 - (1 - \frac{3M}{r_s}) + \sqrt{9 - 6(1 - \frac{3M}{r_s})}\right)\left(3 - (1 - \frac{3M}{r_O}) + \sqrt{9 - 6(1 - \frac{3M}{r_O})}\right)}\right]$$

Finally, we have

$$b_n = 3\sqrt{3}M\left[1 + 216\left(1 - \frac{3M}{r_s}\right)\left(1 - \frac{3M}{r_O}\right)\right.$$
$$\left.\frac{e^{-\left(n+\frac{1}{2}\right)\pi}}{\left(2 + \frac{3M}{r_s} + \sqrt{3 + \frac{18M}{r_s}}\right)\left(2 + \frac{3M}{r_O} + \sqrt{3 + \frac{18M}{r_O}}\right)}\right]. \tag{7.18}$$

7.4 Gap Parameter

Next, we can obtain the gap parameter, introduced by Aratore, Tsupko and Perlick [Aratore et al. (2024)], which is defined as the relative difference between the radii of two consecutive photon rings, normalized by the radius of the bigger ring

$$\Delta_n = \frac{b_n - b_{n+1}}{b_n}. \tag{7.19}$$

Aratore *et al.* have obtained a range of variability of the gap parameter for various spacetimes by changing the emissive radius r_s from a chosen minimum value to infinity. The minimum radius in the case of Schwarzschild spacetime was chosen to be the Innermost Stable Circular Orbit (ISCO) given by $r_{ISCO} = 6M$. And since beyond the ISCO, Schwarzschild spacetime can have stable timelike circular orbits for any radius, the outer limit for r_s was chosen as infinity.

However, recall from Sec. 3.7 that in the Ernst Spacetime, for a subcritical magnetic field strength $0 < B < B_C$, timelike circular orbits can only exist within the range

$$r_2 < r < r_1.$$

Upon stability analysis, we found that stable timelike circular orbits can only be found in the range

$$r_{\text{stable}} \in (r_{\text{ISCO}}, r_1),$$

where r_{ISCO} lies between in (r_2, r_1). Thus, this range defines the disc for which we need to evaluate the gap parameter Δ_n for the given B.

$$r_s \in (r_{\text{ISCO}}, r_1). \tag{7.20}$$

7.4.1 Gap Parameter Intervals

Thus, for a given B value, we can evaluate the range of variability of the gap parameter for the Ernst spacetime. This is given by Fig. (7.1). $B = 0$ is the Schwarzschild case and here $r_s \in (6M, \infty)$ for $r_O = \infty$ to match with the results obtained by Aratore, Tsupko and Perlick [Aratore et al. (2024)]. From Fig. (7.1) we can see that beyond a certain

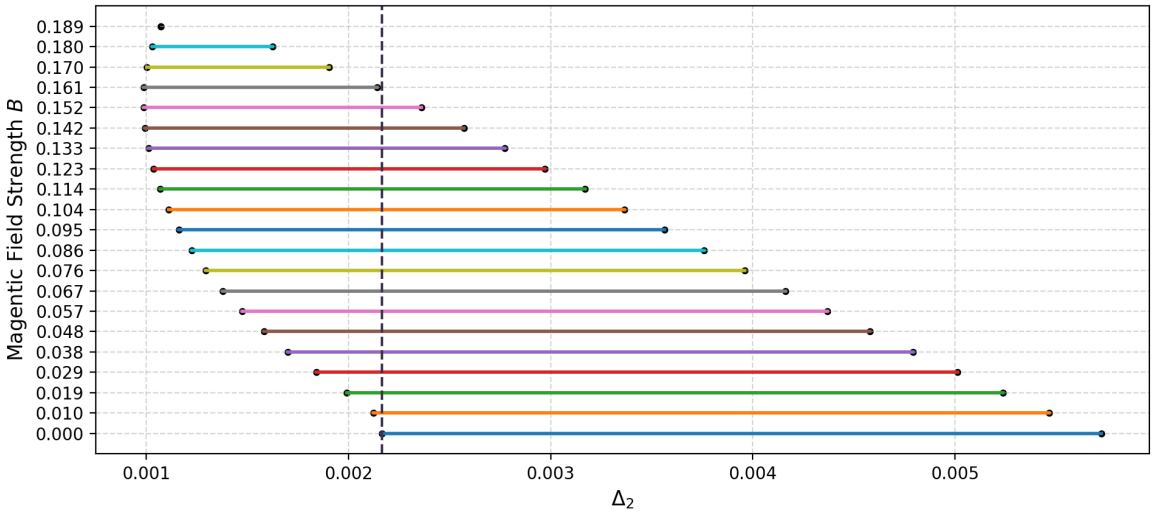

Figure 7.1: Intervals of the gap parameter Δ_2, which is relative separation between $n = 2$ and $n = 3$ photon rings, for the different values of magnetic field strength B in Ernst spacetime. Each line segment shows Δ_2 as r_s varies from the ISCO up to r_1 (outer photon orbit). The last line is the Schwarzschild case ($B = 0$) while the top line is the critical case ($B_c = 0.189/M$). The vertical dashed line separates the Schwarzschild case from the Schwarzschild-Melvin cases with $B > 0.160/M$.

value of magnetic field strength B, the overlap between the range of gap parameter for the Schwarzschild-Melvin case and the Schwarzschild case is null. This corresponds to the case when $r_1 < 6M$ with $r = 6M$ being the ISCO for the Schwarzschild case. One determines this limit numerically to be $B \approx 0.160/M$. This threshold is consistent with the analysis of Aratore, Tsupko and Perlick Aratore et al. (2024), who demonstrated that the gap parameter Δ_n is independent of the black hole mass and observer distance, making it a robust discriminator of spacetime geometry. In particular, for $B \gtrsim 0.160/M$ the allowed range of Δ_2 no longer overlaps the Schwarzschild range. Therefore, if a gap parameter in this range is observed, this observation is incompatible with the assumption that the observed object is a Schwarzschild black hole. It is compatible with the assumption that the spacetime is properly described by the Ernst metric, with a magnetic field $B \gtrsim 0.160/M$. Of course, this conclusion is based on the – not unrealistic – hypothesis that the matter in the luminous disk moves on geodesics.

7.5 Conclusion

We have successfully extended the photon-ring gap parameter formalism to the magnetized Ernst spacetime by exploiting its meridional-plane conformality to Schwarzschild. In doing so, we derived an exact expression for $b_n = (L/E)_n$ valid for a finite observer

at radius r_O. We demonstrated that circular timelike geodesics are restricted to the equatorial plane and exist only in the range $r_2 < r < r_1$, where r_1 and r_2 are the radii of the outer stable and inner unstable null orbits, respectively, reflecting the prohibition of massive particles on photon spheres. An analysis of the second derivative of the effective potential, $V''_{E,L}$, revealed that it is positive only in the interval $(r_{\rm ISCO}, r_1)$, where $r_{\rm ISCO}$ is the innermost stable circular orbit (ISCO). This interval defines a finite disc region for our timelike sources of photon rings. Finally, numerical evaluation of the gap parameter Δ_2 over $r \in (r_{\rm ISCO}, r_1)$ for various values of B illustrates how magnetization modifies the spacing between successive photon rings in comparison to the Schwarzschild case.

Chapter 8

Conclusions and future work

8.1 Summary

In this thesis, we have analyzed the behavior of null geodesics, black hole shadows and photon rings in the Ernst (Schwarzschild–Melvin) spacetime, where a non-rotating black hole is immersed in a uniform magnetic field. Our starting point was the derivation of the conditions for circular lightlike geodesics about the z-axis in the equatorial plane. Imposing $\dot{r} = \ddot{r} = \dot{\theta} = \ddot{\theta} = 0$ leads to a cubic equation whose two positive roots r_1 and r_2 ($r_2 < r_1$) for a sub-critical magnetic field strength ($B < B_c$) correspond to an outer stable orbit r_1 and an inner unstable orbit r_2 [Dhurandhar and Sharma (1983); Esteban (1984)]. In particular, r_2 deforms continuously from the Schwarzschild photon sphere at $r = 3M$ and remains unstable, whereas r_1 is a novel stable lightlike orbit that has no analog in the $B = 0$ limit. At the critical field strength $B = B_c$, the two roots merge and disappear, so that no equatorial photon orbits exist for $B \geq B_c$ inside the event horizon. We further showed that no circular photon orbits about the z-axis can exist off the equatorial plane. Equivalently, we showed that the Ernst spacetime admits no spherical photon orbits with an oscillating θ coordinate. This result contrasts sharply with the Kerr case, where a continuum of non-equatorial spherical photon orbits exists [Teo (2003)].

We also showed that for $B < B_c$ circular timelike geodesics about the z-axis, only exist between the two circular lightlike geodesics and while in the Schwarzschild case, the outer boundary of the stable circular timelike orbits extend to infinity, in the Ernst spacetime, they can only exist between an ISCO and r_1 where ISCO corresponds to the innermost stable circular orbit. While for $B > B_c$, like the circular lightlike orbits, the circular time orbits also cease to exist.

Next, we exploited the fact that Ernst spacetime restricted to $\dot{\phi} = 0$ (constant–ϕ slices) is conformal to Schwarzschild in the meridional plane [Lima Junior et al. (2022)]. Consequently, similar to the Schwarzschild spacetime, each meridional plane contains an unstable photon orbit at $r = 3M$, forming a two-dimensional photon orbit surface that is independent of B. This conformal mapping implies that, in the meridional plane, all shadow and strong-lensing phenomena, such as the divergence of the bending angle near $r = 3M$ and the accumulation of photon rings, follow the standard Schwarzschild formulas, up to a trivial reparametrization.

Using these insights, we derived closed-form expressions for the angular deflection of null geodesics in the meridional plane. The integral δ_{mer} agrees precisely with the

Schwarzschild result and diverges as $r_m \to 3M$. Because the Ernst spacetime is not asymptotically flat, however, one cannot simply subtract π "at infinity" to obtain an exact deflection angle; rather, the expression holds only for observers at a finite radius. In contrast, in the equatorial plane, the presence of the magnetic factor $\Lambda(r, B)$ modifies the effective potential so that any null trajectory with nonzero angular momentum and turning point r_m cannot escape to infinity. Equivalently, the expression under the square root in the equatorial bending integral becomes negative for $r < r_m$, showing that an equatorial light ray passing through a minimum radius cannot return to a distant observer. This extends the result of Dhurandhar et al. [Dhurandhar and Sharma (1983)], who proved that when $B > 0$, no light ray with $L \neq 0$ can reach spatial infinity.

We then computed the angular radii of the black-hole shadow in Ernst spacetime. In the meridional plane, the vertical shadow angle α is identical to Schwarzschild and independent of B. In the equatorial plane, however, the horizontal radius β depends on $\Lambda(r_O, \pi/2)$. In the limit $B \to 0$, β reduces to the Schwarzschild horizontal radius. We explored the different cases of the source radii r_S. We found that for $r_S < r'_O$ where r'_O was identified as a critical observer radius, the constants L/E need to be evaluated at $r = r_2$ for the shadow boundary. However, for the case where $r_S > r'_O$ the value of these critical parameters depends on r_S and hence the horizontal component of the angular shadow radius is a function of the source radius r_S. We showed that in the presence of a magnetic field, the shadow has an oblate geometry, agreeing with the computational findings of Junior et al. [Lima Junior et al. (2022)].

Finally, we examined the structure of photon rings. By applying the strong-deflection expansion [Bozza and Scarpetta (2007)] on each conformal meridional slice, we obtained the expressions for b_n. Finally, following Aratore, Tsupko and Perlick [Aratore et al. (2024)], we plotted the gap parameter between rings of order 2 and 3 for various magnetic field strength B values. We identified that for $B > 0.160/M$ the gap parameter Δ_2 has no overlap with the gap parameter evaluated for the Schwarzschild case. This allows us to characteristically distinguish between the two spacetimes.

8.2 Future Implications

Our results have several important implications. First, the black-hole shadow in the vertical direction is unaffected by the presence of a uniform magnetic field; only the horizontal compression of the shadow reveals $B \neq 0$. This means that one must instead measure both vertical and horizontal shadow diameters, and their ratio β/α is sensitive to B.

Several caveats and future directions remain. First, we assumed a *static, uniform* magnetic field throughout. In realistic astrophysical environments, black holes are more likely embedded in *inhomogeneous* fields (e.g., dipolar or turbulent) and surrounded by *plasma*, which alters photon trajectories via refractive and scattering effects [Perlick et al. (2015)]. Second, we limited our analysis to a *nonrotating* black hole. In a Kerr–Melvin spacetime [Aliev and Gal'tsov (1989); Karas and Vokrouhlický (1991)], meridional conformality no longer holds, so both the critical impact parameter $b_{\rm cr}$ and the gap parameter Δ_n acquire explicit dependence on the spin and magnetic field. Lastly, we evaluated the photon rings for a polar observer $\vartheta_O = 0$. We can analytically extend these results to an arbitrary observer azimuthal angle ϑ_O.

In summary, the Schwarzschild–Melvin solution provides a valuable toy model for exploring how a uniform magnetic field modifies null geodesic structure. We find that, although the functional form of b_n and the vertical shadow radius remain identical to Schwarzschild, the physical gap–parameter distributions differ because stable emission is limited to $r < r_1(B)$ rather than extending to infinity. Moreover, it must be pointed out that in the Schwarzschild spacetime, while stable timelike geodesics cannot exist inside the ISCO, factors like viscosity and pressure can lead these emitters to exist inside the ISCO and can hence give the impression of magnetic field strength $B > 0.160/M$. To mitigate this degeneracy, one must combine gap parameter measurements with independent diagnostics (such as the shadow oblateness $\beta > \alpha$) to unambiguously imply the presence of a magnetic field.

Bibliography

Aliev, A. N. and Gal'tsov, D. V. (1989). "magnetized" black holes. *Soviet Physics Uspekhi*, 32(1):75–92.

Aratore, F., Tsupko, O. Y., and Perlick, V. (2024). Constraining spherically symmetric metrics by the gap between photon rings. *Physical Review D*, 109(12):124057.

Bonnor, W. B. (1954). The magnetic curvature of space-time. *Proceedings of the Physical Society, Section A*, 67(3):225.

Bozza, V. and Scarpetta, G. (2007). Strong deflection limit of black hole gravitational lensing with arbitrary source distances. *Physical Review D*, 76(8):083008.

Claudel, C.-M., Virbhadra, K. S., and Ellis, G. F. R. (2001). The geometry of photon surfaces. *Journal of Mathematical Physics*, 42(2):818–838.

Cunha, P. V. P. and Herdeiro, C. A. R. (2018). Shadows and strong gravitational lensing: a brief review. *General Relativity and Gravitation*, 50:42.

Dhurandhar, S. V. and Sharma, D. N. (1983). Null geodesics in the static Ernst space-time. *Journal of Physics A: Mathematical and General*, 16(1):99.

Duncan, R. C. and Thompson, C. (1992). Formation of very strongly magnetized neutron stars: Implications for gamma-ray bursts. *The Astrophysical Journal Letters*, 392:L9–L13.

Ernst, F. J. (1976). Black holes in a magnetic universe. *Journal of Mathematical Physics*, 17(1):54.

Esteban, E. P. (1984). Geodesics in the ernst metric. *Il Nuovo Cimento B (1971-1996)*, 79(1):76–84.

Gralla, S. E., Holz, D. E., and Wald, R. M. (2019). Black hole shadows, photon rings, and lensing rings. *Physical Review D*, 100(2):024018.

Griffiths, J. B. and Podolský, J. (2009). *Exact Space-Times in Einstein's General Relativity*. Cambridge University Press, Cambridge.

Karas, V. and Vokrouhlický, D. (1991). Kerr black holes in electromagnetic fields. *Journal of Mathematical Physics*, 32(3):714–716.

Kerr, R. P. (1963). Gravitational field of a spinning mass as an example of algebraically special metrics. *Physical Review Letters*, 11:237–238.

Konoplya, R. A. (2003). Magnetized black hole as a gravitational lens. *Physics Letters B*, 564:235–239.

Lima Junior, H. C. D., Cunha, P. V. P., Herdeiro, C. A. R., and Crispino, L. C. B. (2022). Shadows and lensing of black holes immersed in strong magnetic fields. *Physical Review D*, 106(4):044005.

Melvin, M. A. (1964). Pure magnetic and electric geons. *Physics Letters*, 8(1):65.

Perlick, V. (2004). Gravitational lensing from a spacetime perspective. *Living Reviews in Relativity*, 7:9.

Perlick, V., Tsupko, O. Y., and Bisnovatyi-Kogan, G. S. (2015). Influence of a plasma on the shadow of a spherically symmetric black hole. *Physical Review D*, 92(10):104031.

Stephani, H., Kramer, D., MacCallum, M. A. H., Hoenselaers, C., and Herlt, E. (2003). *Exact Solutions of Einstein's Field Equations*. Cambridge University Press, Cambridge, 2 edition.

Teo, E. (2003). Spherical photon orbits around a kerr black hole. *General Relativity and Gravitation*, 35:1909–1926.

Tsupko, O. Y. (2022). Shape of higher-order images of equatorial emission rings around a schwarzschild black hole: Analytical description with polar curves. *Physical Review D*, 106(6):064033.

Acknowledgements

The author acknowledges the support of the generous Erasmus Mundus Master's in Astrophysics and Space Science scholarship. The author also expresses gratitude towards. Dr. Eva Hackmann for kind hospitality at ZARM, University of Bremen.